STUDIES OF STRUCTURAL, PHOTOCATALYTIC AND SHIELDING PROPERTIES OF MXENES SYNTHESIZED BY ETCHING TECHNIQUE

By

Md. Zahid Hasan

Student ID: 21MPHY003P

A thesis submitted in partial fulfillment of the requirements for the degree of

MASTER of PHILOSOPHY

Department of Physics

CHITTAGONG UNIVERSITY OF ENGINEERING & TECHNOLOGY

May 2025

Declaration

I hereby declare that the work contained in this thesis has not been previously submitted to meet the requirements for an award at this or any other higher education institution. To the best of my knowledge and belief, the thesis contains no materials previously published or another person except where due reference is cited. Furthermore, the thesis complies with the PLAGIARISM and ACADEMIC INTEGRITY regulations of CUET.

Md. Zahid Hasan

Student ID: 21MPHY003P

Department of Physics

Chittagong University of Engineering and Technology (CUET)

Copyright © Md. Zahid Hasan, 2025.

This work may not be copied without permission of the author or Chittagong University of Engineering & Technology.

DEDICATED TO

MY WIFE, SON AND PARENTS

List of Publications

Journal Article

Publication: **M. Z. Hasan**, M. H. Haque, M. A. Ali, M. M. Hossain and M. M. Uddin (2025). "Structural, optical, and photocatalytic efficacy of Ti_3C_2 and M2C (M = Ti, V, Cr, Nb) MXene materials synthesized by etching technique", **AIP Advances,** 15, 035334 (2025) https://doi.org/10.1063/5.0251436

Conference Participation

Conference: **M. Z. Hasan**, M. M. Hossain, M. A. Ali, N. I. Khan and M. M. Uddin, "Efficient MXenes photocatalysts for the organic dye degradation under UV and solar light synthesized by etching technique" International Conference on Physics – 2024 organized by Bangladesh Physical Society, Bangladesh Atomic Energy Commission, Dhaka.

Declaration by the Supervisor

This is to certify that Md. Zahid Hasan, Student ID: 21MPHY003P has carried out this research work under my supervision and, he has fulfilled the relevant Academic Ordinance of Chittagong University of Engineering and Technology so that he is qualified to submit the following Thesis in the application for the degree of MASTER of PHILOSOPHY in Physics. Furthermore, the Thesis complies with the PLAGIARISM and ACADEMIC INTEGRITY regulations of CUET.

_____

Dr. Md. Mohi Uddin
(Supervisor)
Professor
Department of Physics
Chittagong University of Engineering and Technology (CUET)

Acknowledgment

First and foremost, all praise to the *Almighty*, the most Beneficent, and the most Merciful, who led me through this research and sustained me with help, guidance, and the power to complete this.

I am extremely delighted to express my deepest sense of gratitude and honor to my supervisor Dr. Md. Mohi Uddin, Professor, Department of Physics, Chittagong University of Engineering & Technology. Your invaluable guidance, support, and encouragement throughout this research journey. Your expertise, patience, and insightful feedback have been instrumental in shaping this thesis and my growth as a researcher. I am truly grateful for the time and effort you dedicated to helping me navigate the challenges of this project, and for inspiring me to strive for excellence. Thank you for believing in my potential and for providing me with the opportunity to explore my academic interests under your mentorship.

I am pleased to express my deep appreciation to Professor Dr. H. M. A. R. Maruf, Head of the Department of Physics, CUET for his official support, continuous help and valuable scientific discussions during this work and opportunity to provide the lab facilities.

I also express highly thanks to my other colleagues Prof. Dr. Mohammad Belel Hossen, Prof. Dr. Swapan Kumar Roy, Prof. Dr. Md. Ashraf Ali, Prof. Dr. Animesh Kumer Chakraborty, Prof. Dr. Nusrat Jahan, Dr. Md. Mukter Hossain, Dr. Shaiful Kabir, Mosammat Arjumanara Bagum, Md. Abdul Jalil for their constant support and encouragement.

I wish to thank specially to my beloved wife and colleague Sinthia Binte Kholil, Lecturer, Department of Physics, CUET for her continuous support during this research work.

I am grateful to the authority of CUET, Chittagong, Bangladesh for giving the necessary permission, financial and technical support during this work for her help during this study.

I would like to thank Md. Sohel Rana, Technical Officer, Department of Physics, CUET for his continuous support during this research work.

Abstract

The etching process was used to synthesized the MXenes (Nb_2C, Ti_2C, Ti_3C_2, Cr_2C, and V_2C) utilizing their respective predecessors, MAX phases Nb_2AlC, Ti_2AlC, Ti_3AlC_2, Cr_2AlC, and V_2AlC. The surface morphology and structural characteristics of the material were examined using scanning electron microscope (SEM) and X-ray diffraction (XRD). The SEM pictures are used to corroborate the layer architectures of the MXenes. The estimated bandgaps range from 1.76 to 1.81 eV, aligning with published values and suitable for light interaction and photodegradation processes. The FTIR analysis further validates the functional group of the synthesized MXenes. Higher degradation efficiencies of 96, 94, and 75% within 120, 160, and 160 minutes are demonstrated by Nb_2C, Ti_2C, and Ti_3C_2. The etching of Al from the Nb_2AlC, Ti_2AlC, and Ti_3AlC_2 MAX phases leads to enhanced surface area, which improves the photodegradation performances. The findings align with the SEM pictures, which unequivocally demonstrate the strong gaps formed by etching the middle layer of their predecessor MAX phases. As a result, Nb_2C, Ti_2C, and Ti_3C_2 MXenes can be suggested as a very efficient and rapid catalyst to address significant environmental pollution issues. In this study, a theoretical investigation was done for the radiation shielding capabilities of MXene materials using the Monte Carlo simulation method. Here we use gamma radiation sources as ^{137}Cs and we get preventing dose rate by MXene materials in the range 19.6 to 8.8 mSv\h.

বিমূর্ত

Nb_2C, Ti_2C, Ti_3C_2, Cr_2C এবং V_2C MXene পদার্থসমূহ ইচিং প্রক্রিয়ার মাধ্যমে সংশ্লেষণ করা হয়েছে, যেখানে তাদের পূর্বসূরি MAX যৌগ —Nb_2AlC, Ti_2AlC, Ti_3AlC_2, Cr_2AlC এবং V_2AlC—থেকে অ্যালুমিনিয়াম অপসারণ সম্পন্ন করা হয়েছে। উপকরণগুলোর কাঠামোগত বিন্যাস ও পৃষ্ঠের গঠন বিশ্লেষণের জন্য এক্স-রে ডিফ্র্যাকশন (XRD) এবং স্ক্যানিং ইলেক্ট্রন মাইক্রোস্কোপি (SEM) ব্যবহার করা হয়। SEM চিত্রসমূহ MXene-এর স্তরযুক্ত বিন্যাস স্পষ্টভাবে প্রতিফলিত করে, যা MAX যৌগ থেকে অ্যালুমিনিয়াম অপসারণের পর সৃষ্ট 2D MXene গঠন তৈরি হয়।

প্রাপ্ত ব্যান্ডগ্যাপের মান 1.76–1.81 eV পরিসরে অবস্থান করছে, যা পূর্বে প্রকাশিত তথ্যের সঙ্গে সামঞ্জস্যপূর্ণ এবং আলো–দ্রব্যের কার্যকর মিথস্ক্রিয়া ও ফটোডিগ্রেডেশন প্রক্রিয়ার জন্য যথোপযুক্ত বলে মনে হয়। ফুরিয়ার ট্রান্সফর্ম ইনফ্রারেড (FTIR) স্পেক্ট্রোস্কোপি সংশ্লেষিত MXene-এর কার্যকরী ফাংশনাল গ্রুপ উপস্থিতি সুদৃঢ়ভাবে নিশ্চিত করে, যা তাদের রাসায়নিক সক্রিয়তার প্রমাণ বহন করে।

ফটোডিগ্রেডেশন পরীক্ষায় প্রাপ্ত ফলাফলগুলোর মধ্যে দেখা যায় Nb_2C, Ti_2C এবং Ti_3C_2 যথাক্রমে 120, 160 এবং 160 মিনিটের মধ্যে 96%, 94% এবং 75% ডিগ্রেডেশন হয়েছে। এ ধরনের উচ্চ কর্মক্ষমতার মূল কারণ হলো MAX পর্যায় থেকে অ্যালুমিনিয়াম অপসারণের ফলে পৃষ্ঠের ক্ষেত্রফলের উল্লেখযোগ্য বৃদ্ধি, যা SEM চিত্রে দৃশ্যমান সুগঠিত আন্তঃস্তর ফাঁকগুলোর মাধ্যমে প্রতিফলিত হয়েছে।

এই ফলাফলগুলো Nb_2C, Ti_2C এবং Ti_3C_2 MXene-কে দ্রুত ও কার্যকর অনুঘটক হিসেবে পরিবেশগত দূষণ সমস্যার সম্ভাবনাময় সমাধান হিসেবে উপস্থাপন করে। তদুপরি, মন্টে কার্লো সিমুলেশন পদ্ধতি ব্যবহার করে তাদের বিকিরণ প্রতিরোধ ক্ষমতার একটি তাত্ত্বিক অনুসন্ধান করা হয়েছে। ^{137}Cs গামা বিকিরণ উৎস হিসেবে ব্যবহার করে দেখা যায়, MXene পদার্থসমূহ 19.6 থেকে 8.8 mSv/h পরিসরে প্রতিরক্ষামূলক ডোজ হার প্রদান করতে সক্ষম, যা বিকিরণ সুরক্ষায় তাদের সম্ভাবনাময় প্রয়োগ নির্দেশ করে।

Table of Contents

Declaration of Candidate		II
Declaration by the Supervisor		V
Acknowledgments		VI
Abstract		VIII
বিমূর্ত		IX
Table of Contents		X
List of Figures		XIII
List of Tables		XIV
Nomenclature		XV
CHAPTER 1	**Introduction**	**1-15**
1.1	Basic concept	1
1.2	Literature review	4
1.3	Motivation	13
1.4	Aim of the present work	14
1.5	Agreement of this thesis	15
CHAPTER 2	**MXenes Preparation**	**16-17**
2.1	Chemicals	16
2.2	Synthesis Procedure of MXenes from MAX Phase	16

CHAPTER 3 Experimental Techniques and Theoretical Aspects 18-32

3.1 Structural and Morphological characterization techniques 18

3.1.1 X-ray diffraction (XRD) 18

3.1.2 Scanning Electron Microscope (SEM) 20

3.1.3 Fourier Transform Infrared Spectroscopy (FTIR) 21

3.2 Optical and Photocatalytic measurements 22

3.2.1 UV-visible spectrometer 23

3.2.2 Photocatalytic activity test 24

3.3 Monte Carlo simulation 25

3.3.1 Monte Carlo Method vs Deterministic Method 25

3.3.1.1 Introduction to MCNP features 26

3.3.1.2 MCNP geometry 26

3.3.1.3 MCNP input file 27

3.3.1.4 Cell cards 27

3.3.1.5 Surface cards 28

3.3.1.6 Data cards 28

3.3.2 Track Length estimate of cell flux, F4 tally 30

3.3.3 Point detector tally, F5 31

Chapter 4 Results and Discussion 33-50

4.1 Structural Properties 33

4.2	Morphological features	37
4.3	Functional group analysis by FTIR	38
4.4	Photocatalytic Performance	40
	4.4.1 Band Gap	40
	4.4.2 Photocatalytic activity	41
4.5	Shielding analysis by MCNP	44
4.6	Credible mechanism of degradation and review report	47

Chapter 5:	**Conclusions**	**51-52**
5.1	General	51
5.2	Key findings	51
5.3	Practical implication	51
5.4	Suggestions for further research work	52

BIBLIOGRAPHY **53-61**

List of Figures

Fig. No.	Figure Caption	Page No.
2.1	Schematic flowchart of MXenes synthesis process by etching technique.	17
3.1	Rigaku Smart Lab diffractometer (MSD, AECD, Dhaka)	20
3.2	FESEM by JEOL, Japan (Department of NCE, BUET)	21
3.3	FTIR by Perkin Elmer (Department of Physics, CUET)	22
3.4	Schematic diagram of a double beam UV-vis spectrometer	23
3.5	UV-vis spectrometer (LAMBDA 365) by Perkin Elmer-USA (Department of Physics, CUET).	24
3.6	Diagram of representation of the particle flux	31
4.1	XRD profile of various MXenes materials	33
4.2	The Williamson-Hall (W-H) plot with linear fitting	36
4.3	The computed crystallite size by theoretical formula and W-H plot for the studied MXenes	37
4.4	SEM images of various MXenes materials synthesized by etching technique.	38
4.5	FTIR images of various MXenes materials	39
4.6	Tauc's plot for measuring the band gap of MXenes materials	41
4.7	(a-e) Wavelength dependent absorption curves of the studied MXenes. (f) photodegradation efficiency of various MXenes 2D materials. (g) time constant of different MXenes materials	43
4.8	Geometry of experimental set up	44
4.9	Schematic diagram of photocatalytic process of MXenes materials	47

List of Tables

Table	Table Caption	Page
1.	Structural parameters of five different MXenes samples	36
2.	Measurement of dose rate shielded by MXene materials using MCNP	45
3.	Comparative summary of the available MXenes materials and obtained results for the photodegradation efficiency of MB	49

Nomenclature

1. Symbols

- d_{hkl}: Interplanar spacing between crystallographic planes
- θ: Bragg angle
- λ: Wavelength of incident X-rays
- n: Order of diffraction
- β: Full width at half maximum (FWHM) of diffraction peaks
- D: Crystallite size
- ε: Microstrain
- $h\nu$: Photon energy
- Eg: Band gap energy
- F(R): Kubelka–Munk function

2. Acronyms and Abbreviations

- **MXenes**: 2D transition metal carbides, nitrides, or carbonitrides
- **MAX Phase**: $M_{n+1}AX_n$ phases, where M = transition metal, A = A-group element, X = C or N
- **HF**: Hydrofluoric acid
- **HCl**: Hydrochloric acid
- **LiF**: Lithium fluoride
- **DI Water**: Deionized water
- **SEM**: Scanning Electron Microscope
- **FESEM**: Field Emission Scanning Electron Microscope

- **XRD**: X-ray Diffraction
- **FTIR**: Fourier Transform Infrared Spectroscopy
- **UV-Vis DRS**: Ultraviolet–Visible Diffuse Reflectance Spectroscopy
- **MCNP**: Monte Carlo N-Particle Code
- **RhB**: Rhodamine B
- **TC-HCl**: Tetracycline Hydrochloride

3. Glossary of Terms

- **Photocatalysis**: Process where light activates a semiconductor to accelerate chemical reactions
- **Band Gap**: Energy difference between the valence and conduction bands determining electronic and optical properties
- **Bragg's Law**: Relationship defining conditions for constructive interference of X-rays in crystals
- **Williamson–Hall Equation**: Method to calculate crystallite size and strain from XRD data
- **EMI Shielding**: Prevention of electromagnetic interference using conductive materials
- **Monte Carlo Simulation**: Statistical method to model particle transport by simulating random interactions
- **In-situ HF Generation**: Safer method to produce HF by mixing LiF and HCl for MXene synthesis

Chapter1: INTRODUCTION

1.1 BASIC CONCEPT

Because of their many uses, 2D materials have attracted a lot of scientific interest. When Michael Naguib of Drexel University discovered MXenes, a novel family of 2D materials distinguished by their remarkable physical, thermal, and chemical characteristics, in 2011, it marked a significant breakthrough in this research[1]. The formula $M_{n+1}X_n$ (where M is an early transition metal and X is carbon or nitrogen) represents the hexagonal close-packed structure of MXenes, which comprise early transition metal carbides, carbonitrides, and nitrides[2]. Their structural resemblance to graphene is reflected in their name. In order to create MXenes, A elements are usually etched from bulk MAX phases using substances like hydrofluoric acid, which leaves surfaces terminated by O, OH, and/or F atoms [3,4]. Numerous MXenes, including those with multiple M elements in solid solutions or ordered phases, have been successfully synthesized, including Ti_2C, V_2C, Mo_2C, Ti_3C_2, and Nb_4C_3 [2]. Furthermore, MXenes' applicability goes beyond solving global issues like water pollution, which offers serious hazards to human and environmental health because of dangerous chemicals, diseases, and heavy metals found in water sources [5]

Furthermore, synthetic dyes are becoming more and more important in a variety of industries, such as the food, cosmetic, tannery, paper, and textile sectors. A sizable amount of the organic matter in the effluents produced by these companies is composed of these hues. Their toxicity, carcinogenicity, and chemical stability make them a serious environmental hazard. Photocatalytic materials aid in the breakdown of pollutants and the release of free radicals because they are exposed to room temperature sunshine. Photocatalytic materials are a highly effective method for addressing environmental and water pollution [6]. Photocatalysis is a process that uses visible or ultraviolet light to activate a

semiconductor oxide catalyst, accelerating chemical reactions like oxidation or reduction [7,8]. The photocatalytic activity of a material is influenced by its surface-to-volume ratio, band gap energy, unique shape, crystal phase, and other unique properties [9]. Metal oxides are widely used as photocatalysts due to their stability, non-harmful nature, and ability to generate charge carriers when exposed to light energy [10–14]. The techniques are discovered to treat the water before releasing it into the environment are adsorption [10–12], precipitation [15], biodegradation [16], solvent extraction [17], membrane separation [18], chlorination [19], ozonation [20], ion exchange [21] and sono-degradation [22]. Photodegradation, a digital catalytic technique, offers numerous advantages including low cost, eco-friendliness, recyclability, and a green process despite its drawbacks like increased premiums and toxic products. Cost, excellent performance, environmental friendliness, and green qualities are just a few advantages of using solar light energy widely for the photocatalytic destruction of certain contaminants.

Numerous semiconductor nanoparticles, including Ti_2O, ZnO, and CdS, have demonstrated significant potential for the degradation of organic contaminants in wastewater [23–25]. Because of its extraordinary chemical and photostability, potent oxidizing power, wide band gap, nontoxicity, and large surface area, Ti_2O is particularly regarded as one of the finest photocatalysts [26,27]. It has been recently demonstrated that the virgin V_2O_5 and 3 mol.% of Yb-doped V_2O_5 samples undergo photodegradation to the extent of 90% and 95%, respectively, after two hours of hydrothermal manufacturing [28,29]. Research on MXene, a family of transition-metal carbides, nitrides, and carbonitrides, focuses on its hydrophilic functional groups, high conductivity, and stability.

Effective electron transfer is made possible by high conductivity in photocatalytic reactions, where electrons must move freely to drive chemical changes. The high

conductivity ensures that photogenerated electrons and holes are efficiently segregated and transported to the material's surface through improved charge carrier mobility. MXenes also have adjustable electronic characteristics because their band gap may be altered by surface functionalization (e.g., adding oxygen, fluorine, or hydroxyl groups) or by changing their chemical composition. They are therefore, suitable for a range of photocatalytic activities that require specific energy levels in order to absorb photons efficiently. Some MXenes can absorb visible light, which broadens the range of light that can be used for photocatalysis compared to many other materials that only respond to UV light. As active sites for photocatalytic reactions, MXene's wide surface area and abundance of functional groups, including -O, -OH, and -F, can enhance the adsorption of molecules like water or organic contaminants and accelerate reaction rates.

These features enable them to function very well in a range of photocatalytic processes, particularly those that include environmental remediation, wastewater purification, water splitting, and visible light absorption [30–32]. Nb_2C MXene exhibits a consistent O-terminated surface and catalytic potential when utilized as a cathode material for Lithium–Oxygen Batteries (LOBs) [33,34]. Furthermore, the potential of composite MXenes for efficient photodegradation is being considered. The hydrothermal treatment of a $TiO_2/Ti_3C_2T_x$ heterostructure has been found to effectively catalyze the degradation of the antiepileptic drug carbamazepine [35–38].

On the other hand, MXenes materials can be used as the EMI shielding materials[39–41]. Several types of shielding including EMI shielding, radiation shielding. Radiation shielding is including ionizing and non-ionizing radiation. Ionizing radiation includes different types of isotopes and non-ionizing radiation includes alpha, beta and gamma radiations.

In this present study, we used Monte Carlo simulation method [42,43] to gives the theoretical study of non-ionizing radiation shielding properties of MXenes materials. Also, synthesize and assess the photocatalytic performance of the MXenes material series and identify effective two-dimensional materials for the removal of pollutants from wastewater and industrial waste.

1.2 LITERATURE REVIEW:

The following are examples of effective photodegradation using composite and MXenes materials:

Alsafari *et al.* 2021 [44] reported the successful synthesis of $CuFe_2O_4$/MXene nanohybrids using a simple ultrasonication method, aiming to improve photocatalytic and antibacterial performance. The $CuFe_2O_4$ nanonuts were found to reduce MXene layer restacking and enhance interfacial contact, resulting in efficient charge separation and increased surface area. The composite demonstrated exceptional photocatalytic activity, achieving 94% degradation of methylene blue under visible light within 40 minutes, significantly outperforming the individual components. Additionally, the nanohybrids exhibited strong antibacterial effects against both Gram-positive and Gram-negative bacteria due to reactive oxygen species generation and membrane disruption. These results suggest the potential of $CuFe_2O_4$/MXene nanohybrids for environmental remediation and biomedical applications.

O. Mashtalir *et al.* 2014 [45] investigated the adsorption and photocatalytic behavior of multilayered $Ti_3C_2T_x$ MXene toward organic dyes in aqueous media. The situdy found that $Ti_3C_2T_x$ strongly adsorbs cationic dyes like methylene blue (MB), with adsorption best described by the Freundlich isotherm, indicating heterogeneous surface interactions. Upon exposure to UV light, $Ti_3C_2T_x$ facilitated significant photocatalytic degradation of both cationic (MB) and

anionic (acid blue 80) dyes, suggesting its potential as a photocatalyst. The MXene materials degrade 81% of methylene blue within 5 hours. The degradation efficiency is good in value but it takes huge time to degrade. Structural analysis revealed gradual oxidation of $Ti_3C_2T_x$ in water, forming TiO_2 and titanium hydroxide, which likely contributed to its photocatalytic activity. These findings demonstrate that MXenes possess tunable surface chemistry and promising applications in environmental remediation, particularly in dye adsorption and photodegradation processes.

Wojciechowski et al. 2019 [46] synthesized Ti_2C MXene-based nanocomposites modified with TiO_2 and noble metal (Ag, Au, Pd) or metal oxide (Ag_2O, PdO) nanoparticles to enhance photocatalytic performance. Structural and morphological analyses confirmed the uniform decoration of MXene flakes with metal and oxide nanoparticles, which altered the bandgap energies between 0.90 and 1.34 eV depending on the modifier. The nanocomposites exhibited high photocatalytic efficiency in the degradation of salicylic acid, with Ag-modified MXenes achieving the highest degradation rates (up to 97.1%). Despite similar bandgap values, photocatalytic activity varied significantly based on the type and oxidation state of metal additives, highlighting the influence of interfacial charge transfer and recombination dynamics. The situdy demonstrates the promise of Ti_2C MXenes as platforms for tunable, high-performance photocatalysts in water purification applications.

Cui *et al.* 2021 [47] implement the hydrothermal synthesis of rod-like Nb_2O_5/Nb_2CT_x composites for visible-light-driven photocatalytic degradation of organic pollutants. The composites were prepared by oxidizing 2D layered Nb_2CT_x MXene under hydrothermal conditions, resulting in Nb_2O_5 nanorods uniformly grown on the MXene surface. Structural and morphological analyses confirmed the formation of a pseudohexagonal phase Nb_2O_5 with exposed (001)

facets, which are highly active for photocatalysis. The Nb_2O_5/Nb_2CT_x composites exhibited superior visible-light absorption and charge separation efficiency due to the Schottky junction formed between Nb_2O_5 and Nb_2CT_x, facilitating electron transfer and reducing recombination.

Photocatalytic tests demonstrated exceptional degradation efficiencies of 98.5% for Rhodamine B (RhB) in 120 minutes and 91.2% for tetracycline hydrochloride (TC-HCl) in 180 minutes under visible light. The enhanced performance was attributed to the composite's high specific surface area (14.075 m^2/g), small pore size (~10 nm), and the synergistic effect between Nb_2O_5 and Nb_2CT_x. The Nb_2CT_x acted as an electron sink, prolonging carrier lifetime, while the Nb_2O_5 nanorods provided abundant active sites for pollutant adsorption and degradation.

Mechanistic studies revealed that holes (h^+) and superoxide radicals ($\bullet O_2^-$) were the primary active species, with hydroxyl radicals ($\bullet OH$) playing a secondary role. The composite's stability was confirmed through five-cycle tests, retaining 87.6% efficiency for RhB degradation. The study highlights the potential of MXene-derived composites for environmental remediation, offering a scalable and efficient approach to degrade organic pollutants. Future work could explore optimizing the hydrothermal conditions to further enhance photocatalytic performance and expand applications to other contaminants.

Xu *et al.* 2024 [48] explores the synthesis and application of a g-C_3N_4@V_2C MXene photocatalyst for enhanced visible-light photocatalytic degradation of methyl orange (MO). The study highlights the challenges of charge transfer and carrier recombination in semiconductor photocatalysts and proposes V_2C MXene as an effective cocatalyst to address these issues. The composite exhibited a 94.5% degradation efficiency of MO, 1.56 times higher than pure g-C_3N_4, attributed to improved electron transfer and reduced recombination. Characterization techniques, including SEM, HRTEM, XRD, and XPS, confirmed the successful integration of V_2C MXene with g-C_3N_4, forming a closely connected interface. The

photocatalyst demonstrated excellent stability, retaining over 85% efficiency after three cycles. Radical trapping experiments identified superoxide radicals ($\cdot O_2^-$) as the primary active species. The band structure analysis revealed a Z-scheme mechanism, where V_2C MXene acted as an electron acceptor, enhancing charge separation. The study positions V_2C MXene as a promising, non-precious cocatalyst for environmental remediation. Comparisons with other g-C_3N_4-based photocatalysts underscored its superior performance. The work provides insights into designing efficient photocatalysts for pollutant degradation under visible light.

Othman *et al.* 2021 [49] investigates the photocatalytic degradation of methylene blue (MB) and rhodamine B (RhB) using AgNPs/TiO_2/$Ti_3C_2T_x$ MXene composites under UV and solar light. The composites were synthesized via a hydrothermal method, where $Ti_3C_2T_x$ MXene served as a substrate for TiO_2 and Ag nanoparticles (AgNPs). Characterization techniques, including SEM, TEM, XRD, and XPS, confirmed the successful formation of the composites, with AgNPs enhancing light absorption and charge separation. The AgNPs/TiO_2/$Ti_3C_2T_x$ composite exhibited superior photocatalytic performance, achieving 99% MB degradation under UV light and 83% under solar light, attributed to the synergistic effects of TiO_2's oxidative properties and AgNPs' plasmonic resonance. The composite also demonstrated stability and efficiency in real wastewater treatment, reducing total organic carbon by 23%. Radical trapping experiments identified superoxide radicals ($\cdot O_2^-$) as the primary active species. The sitady highlights the role of Schottky junctions and surface plasmon resonance in improving charge separation and photocatalytic activity. Comparisons with other photocatalysts underscored the composite's superior performance. This work advances the application of MXene-based materials for environmental remediation, offering a scalable solution for organic dye degradation. The findings suggest potential for broader use in wastewater treatment under natural sunlight.

Zeynep Kalaycloglu *et al.* 2023 [50] stated that a novel ternary composite hydrogel comprising cerium oxide nanoparticles (CeO_2-NPs), graphene oxide (GO), and polyacrylamide (PAM) was synthesized to enhance photocatalytic degradation of methylene blue (MB) dye from aqueous solutions. The composite was characterized by XRD, FTIR, SEM, and UV-vis spectroscopy, confirming successful incorporation of CeO_2 and GO into the hydrogel matrix. Photocatalytic performance was optimized under UV-A light, pH 12, and 5 mg/L MB concentration, achieving 90% degradation within 90 minutes, and demonstrating pseudo-first-order kinetics. Radical scavenging tests revealed that superoxide ($\bullet O_2^-$) and hydroxyl ($\bullet OH$) radicals were primarily responsible for the degradation mechanism. Importantly, the hydrogel showed good reusability, retaining 75% of its photocatalytic efficiency after nine cycles, indicating its promise for sustainable wastewater treatment applications.

Cui *et al.* 2019 [51] stated that the synthesis of 2D/2D Bi_2WO_6/Nb_2CT_x MXene hybrid nanosheets via a hydrothermal method, demonstrating enhanced visible-light-driven photocatalytic activity for degrading organic pollutants like RhB, MB, and TC-HCl. The Nb_2CT_x MXene acts as an efficient co-catalyst, improving charge separation and transfer, which significantly boosts the photocatalytic performance of Bi_2WO_6. The hybrid nanosheets achieved degradation efficiencies of 99.8%, 92.7%, and 83.1% for RhB, MB, and TC-HCl, respectively, with rate constants up to 2.8 times higher than pristine Bi_2WO_6. Characterization techniques confirmed the formation of a Schottky junction at the Bi_2WO_6/Nb_2CT_x interface, reducing electron-hole recombination. This work highlights the potential of MXene-based composites in environmental remediation and water purification.

Shi *et al.* 2019[52] stated that Visible-light-driven photocatalysis using hetero structured semiconductors has gained attention for environmental remediation, particularly in improving charge separation efficiency. $BiVO_4$ is a promising

photocatalyst due to its narrow band gap (~2.4 eV), but it suffers from poor charge transport and rapid recombination of photogenerated carriers. TiO_2, commonly used to enhance $BiVO_4$-based systems, suffers from lattice mismatch with $BiVO_4$ due to structural differences, limiting interfacial charge transfer. To overcome this, the authors introduced a novel TiO_2/C/$BiVO_4$ ternary heterostructure using Ti_3C_2 MXene as a 2D-carbon precursor to bridge TiO_2 and $BiVO_4$.

Phosphate modification was employed to promote chemical bonding and interface compatibility between the components, and Ti_3C_2 was in situ oxidized to TiO_2/C under hydrothermal conditions. Characterizations including XRD, Raman spectroscopy, TEM, and XPS confirmed the formation of intimate heterojunctions and the presence of conductive carbon layers. The ternary composite showed significantly enhanced photocatalytic performance for Rhodamine B degradation under visible light, achieving ~93% removal with a rate constant of 13.7×10^{-3} min^{-1}—about 4× higher than $BiVO_4$ alone. Optical and electronic analyses revealed that the TiO_2/C/$BiVO_4$ system forms a type-II band alignment, enabling effective charge separation and extended light absorption. The 2D-carbon layer not only increased surface area (by ~67%) but also facilitated electron mobility, further reducing charge recombination. This study demonstrates the promising potential of MXene-derived carbon in designing efficient, visible-light-responsive photocatalytic systems for environmental applications.

Long *et al.* 2021 [53]stated that the increasing discharge of dye pollutants in wastewater has led to the development of advanced materials for simultaneous adsorption and photocatalytic degradation. Metal-organic frameworks (MOFs), particularly Fe-based ones like NH_2-MIL-88B(Fe), have been widely studied due to their porous structure and inherent Fenton-like catalytic activity. However, the photocatalytic efficiency of MOFs alone is limited by poor charge separation and

agglomeration. MXenes, such as Ti_3C_2, offer high conductivity and surface functionality but lack direct photocatalytic activity due to their metallic nature. In this study, a novel composite of Ti_3C_2 MXene and NH_2-MIL-88B(Fe) was synthesized via solvothermal in-situ growth to create a Schottky-type heterojunction for enhanced performance. Characterizations confirmed uniform growth of MOF on MXene, reduced agglomeration, increased surface area (~92 m^2/g), and effective charge separation. The composite (especially 0.25-MXene/NH_2-MIL-88B) exhibited strong adsorption (61.82% of MB in 30 min) and high visible-light-driven photocatalytic activity, removing 96.8% of methylene blue within 30 minutes in the presence of H_2O_2. Photocatalytic degradation followed pseudo-first-order kinetics and was enhanced by the synergistic Fenton effect from Fe(III)/Fe(II) cycling. The composite also effectively degraded other dyes such as RhB and MO, though performance was lower due to their complex structures. This work demonstrates a promising integrated adsorbent–photocatalyst for efficient dye removal, leveraging MXene's conductivity and MOF's porosity and Fenton chemistry.

Han *et. al.* 2020 [54] expressed in his paper that the study systematically evaluates the EMI shielding performance of 16 different MXene compositions—including single-metal, ordered double-metal carbide, and solid-solution types—making it the broadest comparative study to date. Ultrathin MXene films were fabricated via techniques such as spin-casting, spray-coating, and vacuum-assisted filtration, spanning thicknesses from nanometers to several micrometers. All tested MXenes exceeded 20 dB in shielding effectiveness (SE) when formed into micrometer-thick films, meeting practical EMI protection standards. Remarkably, a spray-coated $Ti_3C_2T_x$ film just ~40 nm thick achieved an SE of 21 dB, showcasing the material's potential for ultrathin shielding applications. Solid-solution MXenes demonstrated tunable EMI performance by adjusting elemental ratios, allowing for customizable shielding properties. The study

applied a transfer matrix model to interpret shielding behavior in highly conductive MXenes, although the model failed to accurately describe less conductive samples. Findings suggest that absorption—rather than reflection—is the dominant mechanism in MXene-based EMI shielding, which helps minimize unwanted backscattering. By correlating elemental composition, layer structure, and film thickness, the authors provide clear design principles for next-generation MXene shields. The results confirm that many MXenes beyond $Ti_3C_2T_x$ can offer ultrathin, flexible, and effective EMI protection tailored to specific use cases. Overall, this work paves the way for the rational design of multifunctional EMI shielding films in emerging technologies like 5G and IoT, leveraging the vast MXene material family.

Iqbal *et. al.* 2021 [39] stated that MXenes, a family of 2D transition metal carbides, nitrides, and carbonitrides, possess exceptional electrical conductivity, lightweight nature, tunable surface chemistry, and processability, making them promising for electromagnetic interference (EMI) shielding. EMI shielding performance depends on both intrinsic properties—such as high electrical conductivity and layered morphology—and extrinsic modifications like dielectric inclusions, pores, and structural engineering. Pristine $Ti_3C_2T_x$ MXene films demonstrate outstanding EMI shielding effectiveness (SE), achieving up to 92 dB at micrometer thicknesses, outperforming graphene and metal foils of comparable thickness. Nanometer-thick MXene films (40–55 nm) can achieve >20 dB SE, providing 99% shielding efficiency, critical for 5G and portable electronics. The multilayered structure and surface terminations of MXenes promote absorption-dominated shielding through multiple internal reflections and dipolar polarization losses. Introducing porosity and meta-structures, as in Ti_3CNT_x MXenes, further enhances absorption, with SE values up to 116 dB—among the highest reported for synthetic materials. Theoretical models, including Simon's formula and transfer matrix methods, accurately predict EMI SE at high conductivities but fail to fully capture effects like porosity, dielectric

polarization, and meta-structure-induced enhancements. Factors like electrical conductivity, film thickness, porosity, and surface terminations govern overall shielding, with absorption losses (SEA) being dominant in optimized designs. MXene-polymer composites combine low density and flexibility with high SE, meeting the demands for lightweight, foldable, and highly effective shielding in advanced electronics. Future research aims to refine theoretical models, explore magnetic MXenes for additional loss mechanisms, and develop scalable, cost-effective fabrication strategies for next-generation EMI shielding applications.

Hao *et. al.* 2025 [55] stated that MXene-based materials have progressed rapidly from fundamental studies to tailored, intelligent EMI shielding solutions. They offer exceptional electrical conductivity, adjustable surface chemistries, and easy processing in solution, enabling high-performance shielding. The review covers developments from 2016–2024, highlighting composites that achieve shielding effectiveness (SE) above 80 dB at ultralow densities (<0.1 g cm^{-3}). Some MXene systems demonstrate extraordinarily high specific shielding efficiency (SSE/t) values exceeding 30,000 dB·cm^2 g^{-1}. It explores both fundamental experimental approaches and intelligent customization via AI-assisted material design platforms. Advances include extending broadband EMI performance into the GHz–THz range, aimed at future 6G communications. Integration of multifunctional systems—such as flexible, lightweight, and thermally or mechanically robust MXene composites—is discussed. AI-driven design tools are enabling rapid optimization of MXene compositions and architectures for targeted EMI properties. The review underscores persistent challenges: balancing performance in EMI, mechanical flexibility, scalability, and cost-effectiveness. It concludes with strategic insights on future directions, including scalable production, integration into advanced electronics, and expanding applications in 6G and intelligent material systems.

From the above literature review we see that, without modification or doping, the degradation efficiency of MXenes materials is extremely low, as the table's data clearly demonstrates. However, following correction, the efficiency significantly rises. For instance, the degradation effectiveness of Nb_2CT_x for RhB dye is only 17%; however, when rod-like Nb_2O_5 is added to Nb_2CT_x, this efficiency increases to 98.5%. Despite improving performance, the remodeling procedure is costly and time-consuming. There has been much research on the well-known MXenes $Ti_3C_2T_x$, Nb_2CT_x, and their composites, but not on TiC, Cr_2C, and V_2C Pristine V_2C shows just 13% photodegradation [56]. MXenes cannot yet be synthesized on a large scale for use in industrial activities due to the enormous quantities of HF needed for the synthesis, which makes it intractable. A notable advance in MXenes synthesis employing the in-situ generation of HF using LiF + HCl instead of direct HF using has largely overcome the limitation of MXenes [4]. It is essential to look at techniques that use the least quantity of material in order to make the process more cost-effective, time-efficient, and degradation-efficient. This study assessed the synthesis and photodegradation efficiency of MXenes materials, including as Ti_3C_2, Ti_2C, Nb_2C, V_2C, and Cr_2C, in addition to their photocatalytic efficacy.

1.3 MOTIVATION

MXenes are a rapidly growing family of two-dimensional transition-metal carbides and nitrides with attractive properties—high electrical conductivity, large surface area and tunable surface chemistry—that make them promising for applications in photocatalysis, electromagnetic/radiation shielding and energy devices. Despite their potential, two practical and scientific challenges limit their wider use: (1) the most common synthesis routes rely on concentrated hydrofluoric acid (HF), which poses severe safety and scalability problems; and

(2) many pristine MXenes display modest photocatalytic activity unless they are modified, doped or converted into composites, which adds cost and processing complexity.

This thesis addresses both challenges. First, it adopts the safer in-situ HF etching route (LiF + HCl) to produce several MXenes (Ti_3C_2, Ti_2C, Nb_2C, V_2C and Cr_2C) from their MAX precursors, thereby reducing direct handling of concentrated HF and improving the practical feasibility of MXene production. Second, it systematically links synthesis, structure and surface chemistry to functional performance by carrying out detailed structural (XRD), morphological (FESEM), chemical (FTIR) and optical (UV–Vis DRS) characterization and by testing photocatalytic activity for methylene blue degradation under visible light. Finally, the work includes a theoretical Monte Carlo (MCNP) study to evaluate the radiation-shielding potential of the synthesized MXenes, providing a preliminary assessment of their suitability for shielding applications.

In short, the motivation of this thesis is to develop a safer, more practical synthesis route for a range of MXenes, to evaluate and explain their photocatalytic performance under visible light, and to explore their potential as lightweight shielding materials — thereby filling gaps in the literature (limited studies on TiC/Cr_2C/V_2C, dependence of activity on synthesis/termination, and scarce comparative shielding data) and advancing MXene applications in environmental remediation and radiation protection.

1.4 AIM OF THE PRESENT WORK

The main objectives of the present research are as follows:

- Preparation of MXenes using in situ-HF by using etching technique.

- Structural characterization of the samples will be examined by the X-ray diffraction (XRD) analysis.
- Surface morphology will be analyzed by the field emission scanning electron microscopy (FESEM).
- Study of chemical bonding of the synthesized sample by Fourier Transform Infrared Spectrometer (FTIR) analysis.
- Study of the optical properties (absorbance, reflectance and bandgap estimation) of the samples using the UV–vis spectrophotometer.
- Radiation shielding properties will be studied by MCNP code.

1.5 AGREEMENT OF THIS THESIS

The arrangement of the thesis is as follows:

- The general introduction of the present study, i.e., MXenes materials and its application from literature reviews, and motivation as well as the aim of the present work is given in chapter one.
- The sample preparation procedures and characterization techniques of the MXenes materials using In-situ HF by etching techniques are described in chapter three.
- Chapter four is devoted to the results and discussion of various measurements of the compositions under study.
- The summery and conclusions of the present work are given in chapter five.

Chapter 2: MXENES PREPARATION

2.1 CHEMICALS

Commercially available Titanium Aluminum Carbide (Ti_3AlC_2), Titanium Aluminum Carbide (Ti_2AlC), Niobium Aluminum Carbide (Nb_2AlC), Vanadium Aluminum Carbide (V_2AlC), Chromium Aluminum Carbide (Cr_2AlC) were collected [Forsman Scientific (Beijing) Co., Ltd, China] without any further purification.

2.2 SYNTHESIS PROCEDURE OF MXENES FROM MAX PHASE

The most widely used synthesis technique involves selective etching of the "A" element from the MAX phase using strong etchants such as hydrofluoric acid (HF) or in situ generated HF (e.g., a mixture of lithium fluoride and hydrochloric acid). This top-down approach leads to the exfoliation of layered MXene nanosheets. Alternative methods, such as molten salt etching, offer a fluorine-free route and provide better control over surface chemistry and layer termination. Additionally, electrochemical etching and hydrothermal methods have been explored to improve safety, scalability, and environmental sustainability. The etching process is a critical step and typically involves immersing MAX phase powder in a chemical etching solution. Hydrofluoric acid (HF) is widely used as an etchant due to its ability to selectively react with the A-layer. Since direct hydrofluoric acid (HF) is bad for human health and requires rigorous technique, as an alternative, safer methods entail the generation of HF in situ by combining hydrochloric acid (HCl) with a fluoride salt, such as lithium fluoride (LiF). So, firstly, 90 milliliters of 12 M hydrochloric acid (HCl) are used to dissolve 6 grams of LiF and 3 grams of MAX phase powder. The mixture is then agitated for 48 hours using a magnetic stirrer. The reaction between the

etchant and the MAX phase removes the aluminum layer as a soluble byproduct, such as AlF_3, while the Ti−C layers remain intact, forming the MXene Ti_3C_2. For example, in the case of Ti_3AlC_2, the reaction can be represented as:

MAX phase materials +in situ-HF → MXenes materials +AlF_3+1.5H_2 …… (1)

Throughout the procedure, the mixture's temperature is kept at 35°C. In the time of synthesis, the room temperature remains in between 33-36^{0}C. After the etching process it needs to be wash the mixture. The washing process begins with the deionized (DI) water. The mixture washed by deionized (DI) water three times. The pH of the solution will be measured by pH meter after each washed process. After that the solution will be washed by HCl twice. Then the solution will be washed by ethanol and water are used to wash the solution until it turns neutral. A centrifuge is used for the washing process, spinning the fluid for 15 minutes at 5500 RPM. To raise the sample's pH to 7, the solution is usually rinsed twice with DI water, once with HCl, and several times with ethanol. The mixture is then dried for eighteen hours at 60 to 70 degrees Celsius. For half an hour, the final product is crushed and ground. Below is a flowchart showing the complete synthesis process:

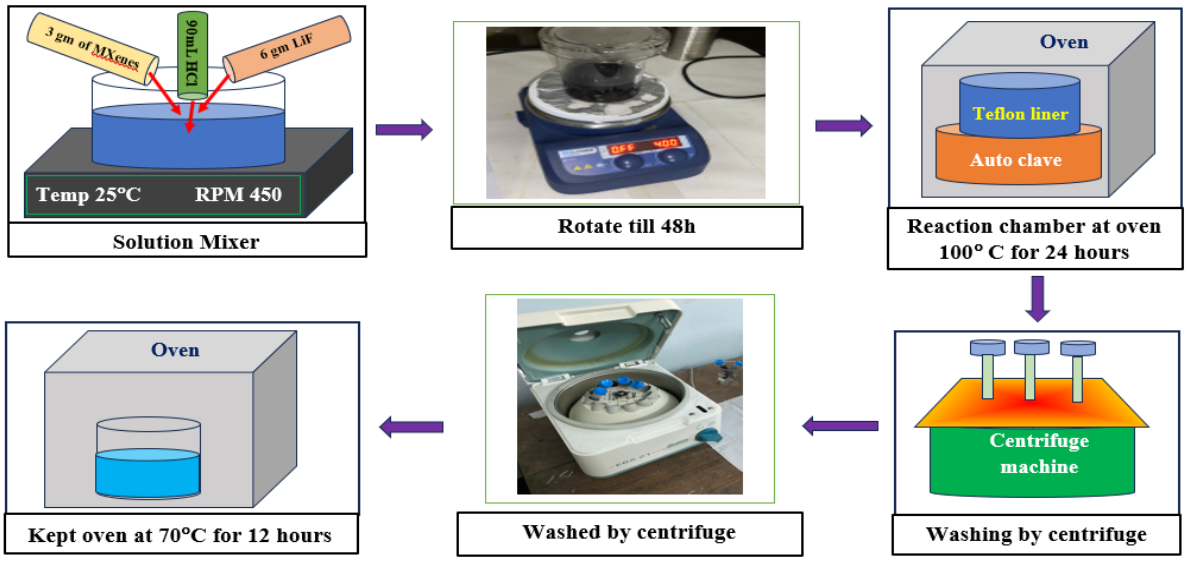


Figure 2.1: Schematic flowchart of MXenes synthesis process by etching technique.

Chapter 3: EXPERIMENTAL TECHNIQUES AND THEORETICAL ASPECTS

3.1 STRUCTURAL AND MORPHOLOGICAL CHARACTERIZATION TECHNIQUES

The structural, morphological, and optical properties of the synthesized samples were assessed through the use of a variety of analytical techniques.

The crystallographic phase and structure were determined using a Rigaku Smart Lab diffractometer with Cu-Kα radiation (λ = 1.5406 Å). X-ray diffraction (XRD) analysis was undertaken. The surface morphology and particle size distribution were analyzed using scanning electron microscopy (SEM) (JEOL, JSM-6010LA).

Fourier-transform infrared spectroscopy (FT-IR) (PerkinElmer) was employed for functional group analysis. Furthermore, the optical bandgap was estimated using UV-Vis diffuse reflectance spectroscopy (DRS) captured on a PerkinElmer LAMBDA 365 spectrophotometer (USA).

3.1.1 X-RAY DIFFRACTION (XRD)

X-ray Diffraction (XRD) is a powerful and widely employed analytical technique used to investigate the structural characteristics of crystalline materials. It provides essential information such as phase identification, lattice parameters, crystal structure, and the average crystallite size—especially significant in the characterization of nanocrystalline substances. This technique is highly versatile and can be effectively applied to a variety of sample types, including solid specimens of different shapes and sizes, powdered samples, and thin films.

When XRD is performed using powdered samples, the technique is referred to as powder X-ray crystallography. This methodology relies fundamentally on

Bragg's Law, which describes the condition for constructive interference of X-rays scattered by the periodic atomic planes within a crystal. The mathematical representation of Bragg's Law is as follows:

$2d_{hkl}\sin\theta = n\lambda$…….(2)

In this equation:

- d_{hkl} represents the interplanar spacing between crystallographic planes indexed by Miller indices (hkl),
- θ is the angle of incidence (also known as the Bragg angle),
- λ is the wavelength of the incident X-rays, and
- n is an integer denoting the order of diffraction.

Bragg's Law forms the theoretical foundation for interpreting diffraction patterns, allowing the determination of crystal structure by analyzing the angles and intensities of the diffracted X-rays.

In the present study, XRD measurements were conducted using a **Rigaku SmartLab X-ray diffractometer**. The experiments were carried out at room temperature, employing **Cu-Kα radiation** with a characteristic wavelength of **1.5405 Å**. The scanning was performed over a 2θ range of **5° to 80°**, with a scan rate of **1° per minute**. This setup enabled high-resolution detection of diffraction peaks, facilitating a precise analysis of the crystal structure and microstructural properties of the particle samples under investigation.



Figure 3.1: Rigaku Smart Lab diffractometer (MSD, AECD, Dhaka)

3.1.2 SCANNING ELECTRON MICROSCOPE (SEM)

A Scanning Electron Microscope (SEM) is an essential tool for analyzing surface morphology. It produces magnified images by directing an electron beam from an electron cannon onto the sample's surface. The interaction between the beam and the sample generates signals that are recorded. The beam is focused to a tiny point (0.4 nm to 5 nm) using two condenser lenses, operating within an energy range of a few hundred eV to 40 keV, leading to energy loss.

The loss of energy is absorbed by the interaction surface of the sample. However, there are special detectors in SEM that detect the high energy electron due to elastic scattering, secondary electrons by inelastic scattering, and also the EM radiations. These signals are amplified by the electronic amplifier. The amplified singles along with the beam current absorbed by the sample are processed to create magnified images of the specimen and then displayed using a monitor. In addition, the characteristics X-ray that are produced due to the ejection of electrons from the inner shell of the sample as primary electrons beam interact

are used to find the composition of the specimen. The surface morphology of the powder samples was studied using JEOL, JSM6010LA at room temperature.



Figure 3.2: FESEM by JEOL, Japan (Department of NCE, BUET).

3.1.3 FOURIER TRANSFORM INFARED SPECTROSCOPY (FTIR)

Fourier Transform Infrared Spectroscopy (FTIR) is a widely used cost-effective and easy analytical method to identify and analyze the vibrational modes in the specimen. In this technique, an inferred light source is employed to scan the solid, liquid, and gas samples. In general, the FTIR spectrum can be recorded from 4000 to 400 cm^{-1}. In a typical FTIR, the molecules of the samples absorbed the energy of proper frequency, and accordingly, molecules get vibrated.



Figure 3.3: FTIR by Perkin Elmer (Department of Physics, CUET).

The frequency that has been absorbed by the specimen can be recorded from the transmitted energy as a function of radiation energy. Now from the transmittance versus wavelength (cm^{-1}), plot one can identify the functional groups of the sample under investigation. In our study, first the KBr powder mix with a sample (250:1), and then a pellet was prepared. The pellet was put into the chamber of FTIR to record the spectrum. We have used Jupiter, STA449 F3 to analyze the vibrational modes.

3.2 OPTICAL AND PHOTOCATALYTIC MEASUREMENTS

The DRS data from UV-vis spectrometry was utilized to estimate the bandgap of synthesized samples. To evaluate their degradation efficacy, the photocatalytic activity of methylene blue (MB) dye was tested using two V_2O_5 samples. This assessment.

3.2.1 UV-VISIBLE SPECTROMETER

The UV-vis spectrometer is used to investigate the optical properties of the sample. It can record the absorbance, reflectance, and transmittance of solid, liquid, and thin-film samples. The beam of the spectrometer determines the availability of three distinct varieties of UV-vis spectrometers.

1) single beam spectrometer, 2) double beam spectrometer and 3) simultaneous spectrometer.

In the present work, we used a double beam spectrometer to estimate the bandgap of the synthesized samples.

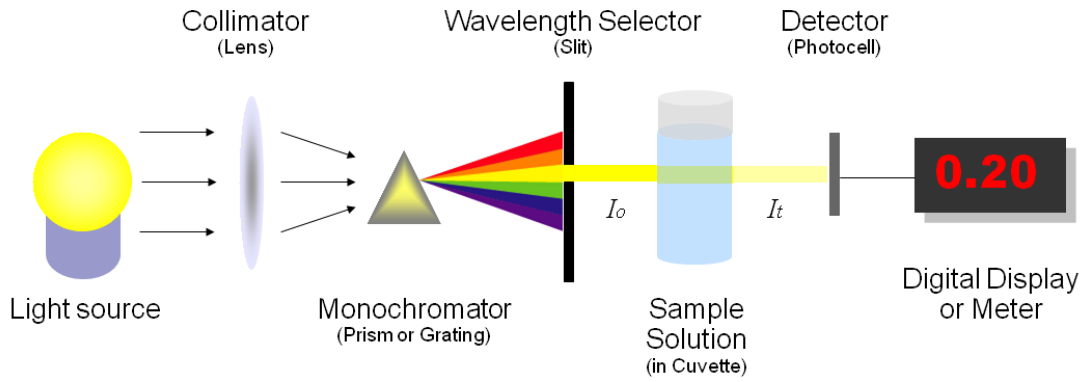


Figure 3.4: Schematic diagram of a double beam UV-vis spectrometer

Figure 3.4 shows the schematic diagram of a double beam UV-vis spectrometer. The diffuse reflectance of the powder samples is recorded using LAMBDA 1050, PerkinElmer-USA spectrometer. First, the sample was mixed well with a perfectly white material $BaSO_4$ and then press hard in the sample holder. Finally, the holder was placed in the chamber of the spectrometer, and the DRS data was recorded to estimate the bandgap of the samples.



Figure 3.5: UV-vis spectrometer (LAMBDA 365) by Perkin Elmer-USA (Department of Physics, CUET).

The bandgap of the pristine V_2O_5 powder samples has been determined using the Kubelka-Munk (K-M) method in this study [57]. The following equation was employed to estimate the bandgap of the sample:

$$F(R_\infty) = \frac{A(h\nu - E_2)^n}{h\nu} \quad (3)$$

The Kubelka-Munk Function is represented by $F(R_\infty) = (1\text{-}R)^2/2R_\infty$, [58]. Consequently, the energy band gap E_g (eV) can be determined by extrapolating the linear portion of the plot to the energy axis, as illustrated by the plot of $[F(R_\infty)h\nu]^2$ Vs photon energy ($h\nu$).

3.2.2 PHOTOCATALYTIC ACTIVITY TEST

The degradation of methylene blue (MB) dye under visible light irradiation was monitored to assess the photocatalytic performance of the synthesized sample. The experimental procedure was implemented in the following manner:

A 25 mL aqueous solution of MB dye (1×10^{-5} M) was prepared by mixing with deionized water for 30 minutes. After adding 5 mg of catalyst, the mixture was agitated in the dark for another 30 minutes to achieve adsorption-desorption

equilibrium. The photocatalytic degradation process began under visible light, with absorbance measured every 20 minutes over 180 minutes. To ensure accuracy, the catalyst was centrifuged for 10 minutes before each measurement, confirming the degradation of MB dye through color change as illustrated in Figure 4.9.

3.3 MONTE CARLO SIMULATION

MCNP is a powerful Monte Carlo radiation transport code that is capable of simulating continuous-energy particle interactions in complex geometries and time-dependent scenarios. It facilitates the tracking of numerous particle types across a broad energy spectrum and simulates complex three-dimensional material configurations that are bounded by first- and second-degree surfaces, as well as fourth-degree elliptical tori. In order to guarantee precise particle transport calculations, pointwise cross-section data are computed for this simulation [59].

3.3.1 MONTE CARLO METHOD VS DETERMINISTIC METHOD

Monte Carlo techniques differ fundamentally from deterministic transport approaches. While deterministic methods solve particle transport equations to model average behavior, Monte Carlo simulations track individual particle histories and statistically infer system-wide behavior through user-defined tallies. By applying the central limit theorem, the aggregated results from numerous simulated particles approximate the expected physical behavior. Unlike deterministic approaches that provide comprehensive solutions, Monte Carlo calculations only generate data for the specific quantities (tallies) selected by the user.

3.3.1.1 INTRODUCTION TO MCNP FEATURES

Some basic MCNP features are described below in brief:

Nuclear Data and Reactions

Livermore's ENF, ENDL, and ACTL compilations are the primary sources of nuclear data for MCNP, along with evaluations from the T-2) Group at Los Alamos, providing continuous energy.

Source Specification

MCNP's user-input source capability allows users to specify various source conditions without code modification, including independent probability distributions for variables like time, position, energy, direction, and initial cell or surface.

Output and Tallies

MCNP provides statistics on particle flux, current, and energy deposition, normalizing tallies per initial particle. It calculates current across surfaces, charges electrons and positrons, and extracts fluxes in cells and across surfaces.

Monte Carlo Error Estimation

The MCNP tallies are normalized per starting particle and output a second number, the estimated relative error, calculated as one estimated standard deviation divided by the estimated mean [60].

3.3.1.2 MCNP GEOMETRY

MCNP offers a more generalized geometry, allowing users to designate geometrical regions from analytical geometry and elliptical tori, combine them with Boolean operators, and conduct internal checks to identify input errors.

3.3.1.3 MCNP INPUT FILE

To simulate desired quantities in MCNP, an input file can be developed manually by inserting coding parameters into the visual editor program.

"Message Block

Blank Line Delimiter

One Line Problem Title Card

Cell Cards

……

Blank Line Delimiter

Surface Cards

……..

Blank Line Delimiter

Data Cards

……..

Blank Line Terminator (optional)"

The main components of the input file are described below in brief.

3.3.1.4 CELL CARDS

Cells are labeled, assigned substance, cell, and material density, with constraints like operators and signed surfaces. Material number can be zero if no material exists.

3.3.1.5 SURFACE CARDS

To bind a cell in MCNP, a suitable surface can be specified using coefficients satisfying the surface equation or known geometrical points on a rotationally symmetric surface.

3.3.1.6 DATA CARDS

To simulate particle transportation, a data card is needed, including neutron, photon, and electron importance. The cards are detailed in mode, cell and surface parameters, simplifying physics, source, tally, material, and problem cutoffs.

MODE Card

The MODE card, omitted when MODE is present, considers neutron-induced photons and lacks photon-production cross sections. MCNP prints warning messages if Mode N P issues are not addressed.

Cell and Surface Parameter Cards

The majority of cell parameter cards in the INP file specify values, with some cards indicating sequence entries. Other cards are for optional variance reduction techniques, necessitating relative cell importances.

Source Specification Cards

The SDEF card is a method for defining beginning particles, specifying fundamental source parameters like commencing cell number and position. It defaults to 0 0 0, 14 MeV, WGT, TME, and PAR, with PAR representing source particle type.

Cards for Simplifying Physics

The PHYSICS card has four parameters for neutrons: PHYS:N, EMAX, EMCNF, IUNR, and DNB. EMAX is the energy in MeV at which neutron data is not stored, IUNR is the energy below the EMCNF, and DNB determines whether v(E) includes prompt and delayed neutrons, prompt neutrons only, or delayed neutrons per fission [60].

Tally Specification Cards

MCNP calculates six standard neutrons, six standard photons, and four standard electron tallies, normalized per initial particle, with distinct normalizations in tallies for criticality calculations.

Tally Mnemonic Description are given below:

"F1:N or F1:P or F1:E Surface current

F2:N or F2:P or F2:E Surface flux

F4:N or F4:P or F4:E Track length estimate of cell flux

F5a:N or F5a:P Flux at a point (point detector)

F6:N or F6:N,P Track length estimate of energy deposition or F6:P F7:N Track length estimate of fission energy deposition

F8:P or F8:E Energy distribution of pulses created or F8:P,E in a detector."

The simulation code utilizes F4 tally for spectroscopic measurement and F5 tally for dosimetric measurement, with detailed descriptions provided.

3.3.2 TRACK LENGTH ESTIMATE OF CELL FLUX, F4 TALLY

The F4 tally represents the average particle flux in a cell, with each particle contributing to the total flux within a cell of volume V [60].

"Let $\psi(\vec{r}, \hat{\Omega}, E, t)$ is the angular flux and it is expressed as

$\Psi(\vec{r}, \hat{\Omega}, E, t) = vn(\vec{r}, \hat{\Omega}, E, t)$; where $n(\vec{r}, \hat{\Omega}, E, t)$ is the particle density (particles/cm^3/MeV/steradian) and v is velocity cm/sh. The scalar flux $\varphi(\vec{r}, E, t)$ is defined by [39]

$$\Phi(\vec{r}, E, t) = \int d\Omega\, \psi(\vec{r}, \hat{\Omega}, E, t) \tag{4.1}$$

The total scalar flux in volume element dV, energy element dE within time dt is given by

$$= \varphi(r, E, t)\, dV\, dE\, dt$$

Introducing energy and time bins, the average flux in a cell can be written as

$$\overline{\phi}_V = \frac{1}{V} \int dE \int dV \int dt \int d\Omega\, \psi(\vec{r}, \hat{\Omega}, E, t)$$

$$= \frac{1}{V} \int dE \int dV \int dt \int d\Omega\ v\, n(\vec{r}, \hat{\Omega}, E, t)$$

$$= \frac{1}{V} \int dE \int dV \int dt\, v\, N(\vec{r}, E, t) \tag{4.2}$$

where $N(\vec{r}, E, t) = \int d\Omega\, n(\vec{r}, \hat{\Omega}, E, t)$ is the density of particles, independent of trajectories, at a point. It is the desired F4 tally. Defining $dT = v\, dt$, differential track length, above equation becomes

$$\overline{\phi}_V = \frac{1}{V} \int dE \int dV \int dT\, N(\vec{r}, E, t)" \tag{4.3}$$

The average flux can be calculated by combining track lengths, as per the F4 tally definition.

3.3.3 POINT DETECTOR TALLY, F5

The point detector next-event estimator estimates neutral particle flux at a point or ring. An array of point detectors can also be used. However, caution is advised as they can produce anomalous statistics. Point detectors are deterministic estimates derived from present event points, contributing to random walk tally [60].

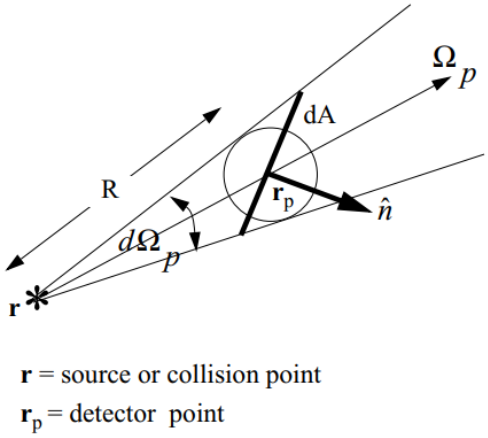


Figure 3.6: Diagram of representation of the particle flux

The particle must scatter toward the solid angle $d\Omega_p$, which occurs with probability upon crossing dA, to contribute to a flux tally, as it is in the direction of the sphere's center. The tally F5 is obtained by the following equation:

$$F5 = w\frac{p(\mu)}{2\pi R^2}e^{-\int_0^R -\Sigma_t(s)ds} \qquad 4.4$$

Therefore, the syntax of F5 tally is as follows:

Fn5:pl $x\ y\ z\ r$

where, n = 0 to 999, x y z are the three coordinates of the midpoint of the detector surface and r is the radius of the detector surface. Here pl stands for the particle type.

Materials Specification

This material specification card provides isotopic composition and cross-section evaluations for materials. It is specified by three quantities: Nuclide Identification Number (ZAID), Nuclide Fraction, and VOID Card. ZAID designates the desired element or nuclide, while fractions can be weight or atomic. The VOID Card recognizes a void in a cell by assigning material number 0 to it.

Problem Cutoffs

This card is utilized to terminate MCNP execution in various ways, setting the nps number to a desired amount (not exceeding 1000000000 in MCNP5) and terminating after specified particle histories.

Cross Sections

The MCNP code consists of eight nuclear data tables, including continuous-energy neutron interaction data, discrete reaction neutron interaction data, photon interaction data, neutron dosimetry cross sections, neutron S(α, β) thermal data, and electron interaction data.

Chapter4: RESULTS AND DISCUSSION

4.1 STRUCTURAL PROPERTIES

The XRD technique was used to analyze the synthesized samples' crystal structure. Fig. 3 displays the XRD patterns of the MXenes powder samples that were prepared under similar circumstances. Every peak in the XRD patterns corresponds to the typical JCPDS card XRD patterns, suggesting that a stable trigonal structure has formed [61]. All of the peaks in the well-researched MXenes Ti_3C_2 agree with its JCPDS card number #52-0875. The JCPSD card numbers of the other MXenes [Ti_2AlC (01-081-8106), Nb_2AlC (30-33), Cr_2AlC (29-0017), and V_2AlC (29-0101)] are likewise matched.

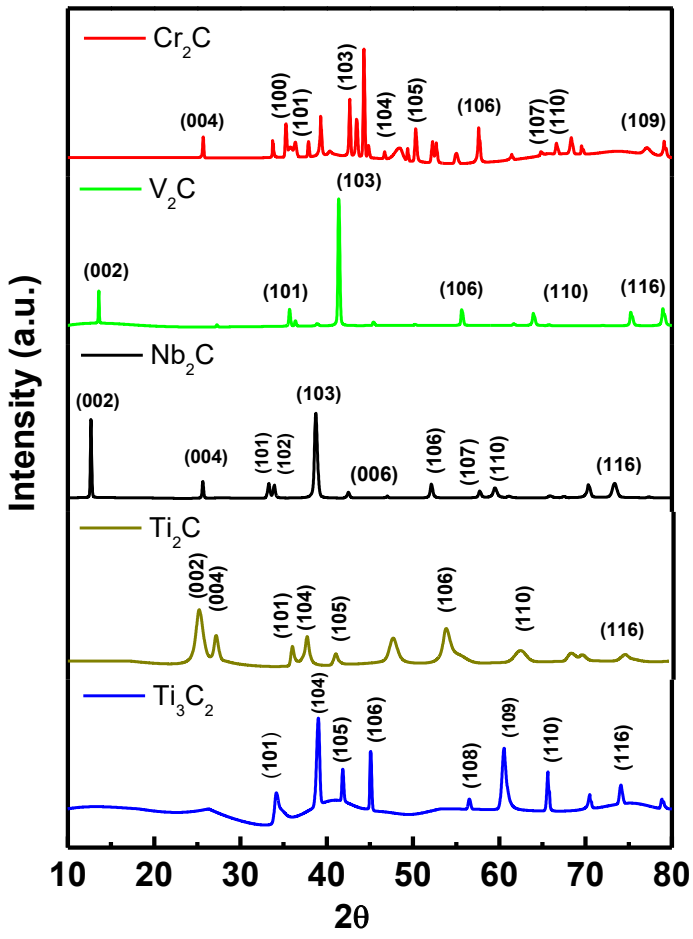


Figure 4.1: XRD profile of various MXenes materials.

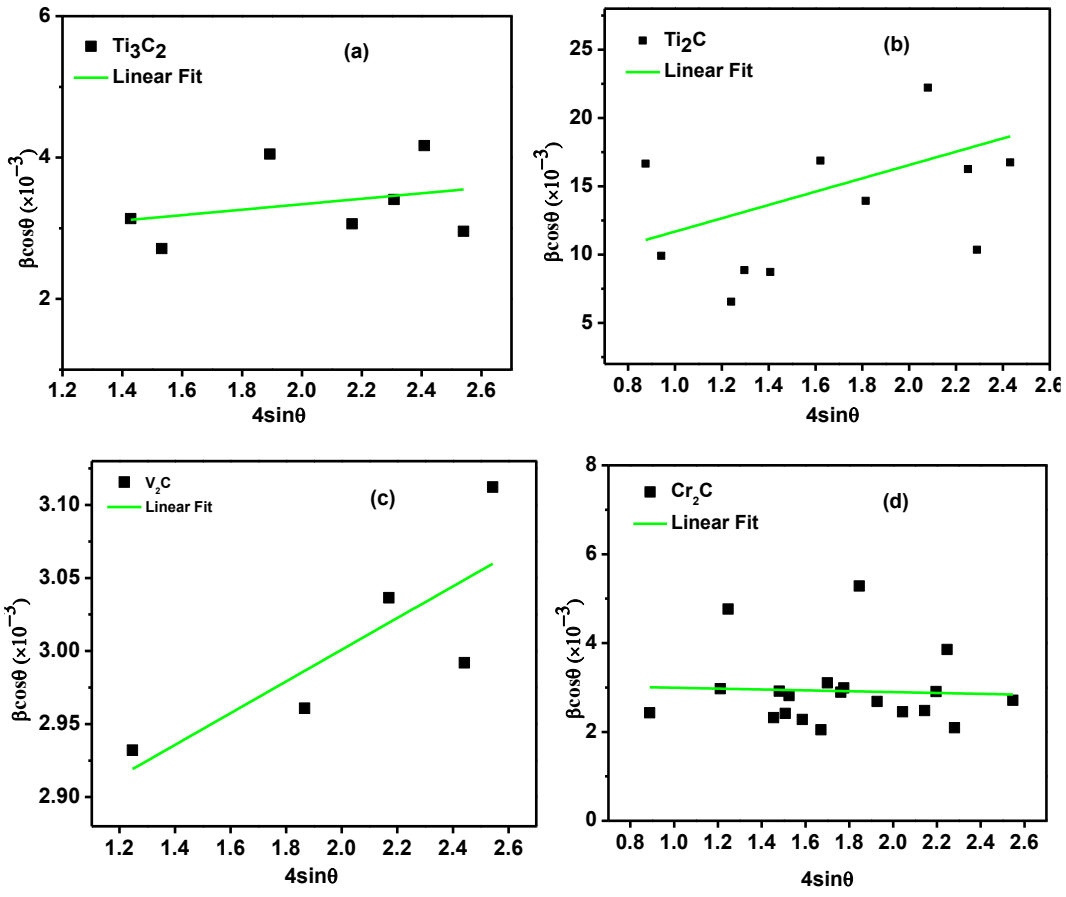
The provided X-ray diffraction (XRD) pattern compares the crystalline structures of five transition metal carbides: Cr_2C, V_2C, Nb_2C, TiC, and Ti_3C_2. Each compound exhibits distinct diffraction peaks that reflect its unique crystallographic structure. Cr_2C (red) shows numerous sharp peaks, especially around 30°–50°, indicating a complex and possibly multiphase structure. V_2C (green) has a dominant (103) peak with fewer secondary reflections, suggesting a simpler, layered hexagonal structure. Nb_2C (black) is characterized by a strong (002) peak and several other well-defined reflections, consistent with a highly ordered, layered structure. TiC (golden) displays sharp, symmetric peaks such as (111), (200), and (220), confirming a highly crystalline cubic rock-salt structure. In contrast, Ti_3C_2 (blue) shows broad and intense (002) and higher-order reflections, which are characteristic of 2D layered MXene structures with expanded interlayer spacing. Overall, this XRD comparison reveals differences in crystallinity, phase composition, and dimensionality, providing valuable insights into the structural nature and potential applications of these carbide materials in areas such as energy storage, catalysis, and coatings

The XRD patterns reveal that the doping samples do not contain secondary phases, as evidenced by the absence of extra peaks. When the examined MXenes' conspicuous peaks are compared to their predecessor MAX phases, the consistency is confirmed. It has been observed that certain phases of Cr_2C are difficult to detect; these might be connected to the magnetic nature of Cr. The mechanism is still being studied and is not fully understood.

The Scherrer equation, which linked the peak broadening (β) to the cryatallite size (D) and the internal lattice strain (ε), was simplified into the Williamson-Hall (W-H) equation (1). The formula is as follows:

$$\beta \cos\theta = \frac{K\lambda}{D} + 4\varepsilon \sin\theta \qquad (4)$$

where k is a dimensionless constant known as the shape factor (value assumed as 0.9), β is the peak's full width at half maximum (FWHM), and θ is the Bragg angle. Fig. 4 shows the W-H plot. Plotting the W-H equation yields a number of crucial factors that may be used to determine the samples' structural properties. Using the slope of the W-H plot, the average crystalline size of the synthesized samples was calculated and appears as follows: D is equal to $D = \frac{0.9\lambda}{\beta \cos\theta}$, where λ is the radiation wavelength and β and θ are the Bragg angle and integral breadth, respectively. The calculation of the dislocation density is $\delta = \frac{1}{D^2}$, where δ is the average crystallographic size and δ is the dislocation density. Table 1 contains the MXenes' computed structural parameters. using $\varepsilon = \frac{\beta}{4\,tan\theta}$, is used to compute the micro strain of the samples, and the results are given in Table 1.



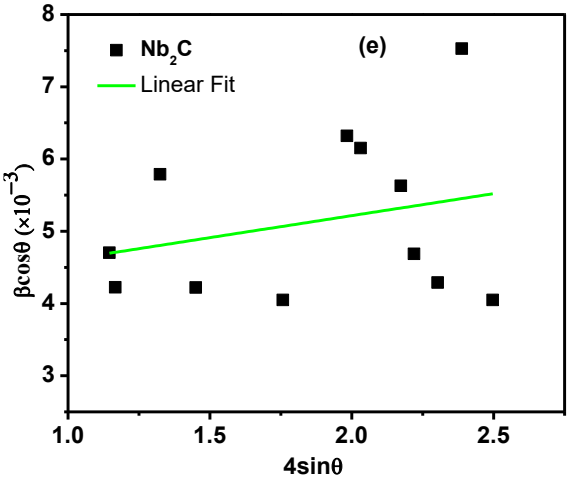


Figure 4.2: The Williamson-Hall (W-H) plot with linear fitting.

The corresponding parameters calculated from the W-H plot is summarized in the table below.

Table-1: Structural parameters of five different MXenes samples.

Sample Name	Crystalline Size, nm	Interplanar spacing	Micro strain	Dislocation Density lines/nm²
Ti_3C_2	35	1.7506	0.0029	0.0015
TiC	11	2.0479	0.0094	0.0141
Nb_2C	36	2.1998	0.0029	0.0011
V_2C	48	2.1929	0.0021	0.0005
Cr_2C	46	1.9282	0.0028	0.0022

Figure 4.3 shows the well-agreed crystalline size of the produced MXenes materials between the calculated and from the W-H plot. It is evident that there are very few differences and that the values are constant. The TiC exhibits a lower crystallite size than the others due to its greater micro strain value.

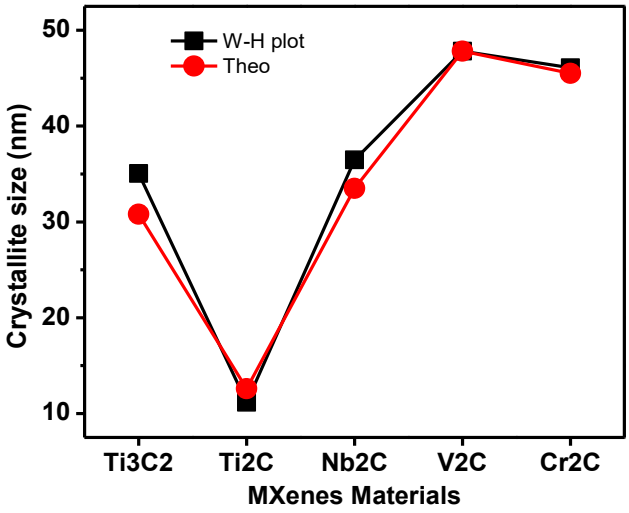


Figure 4.3: The computed crystallite size by theoretical formula and W-H plot for the studied MXenes.

4.2 MORPHOLOGICAL FEATURES

The JSM 7600F and JEOL-Japan FESEM SEM images with ×30k magnifications were used to do the morphological analyses of the MXenes materials under study. There were several layers with strong gaps seen in the SEM pictures. The etching of the Al layer causes the spaces between layers. There are benefits to using these kinds of layer architectures for photocatalytic measurement. Because of the mid-layer etch, layered structures particularly thin films or MXenes are known to offer a significant surface area relative to volume. Increasing the surface area of a material is crucial to boosting its photocatalytic activity since the process of photocatalysis occurs at the surface [31,38]. Custom band gaps that are perfect for absorbing specific light wavelengths can also be added to the 2D materials. Using a layer-by-layer design can increase light absorption across a wide range and improve photodegradation efficiency. A material absorbs light to produce pairs of electrons and holes. Because layered materials facilitate charge separation and inhibit recombination, they can enhance photocatalytic performance. Consequently, MXenes have remarkable photocatalytic properties due to their enormous surface areas and layered structures. Additionally, Fig. 4.4

shows that while the grains in Cr_2C are agglomerated, the remaining MXenes are well-layered.

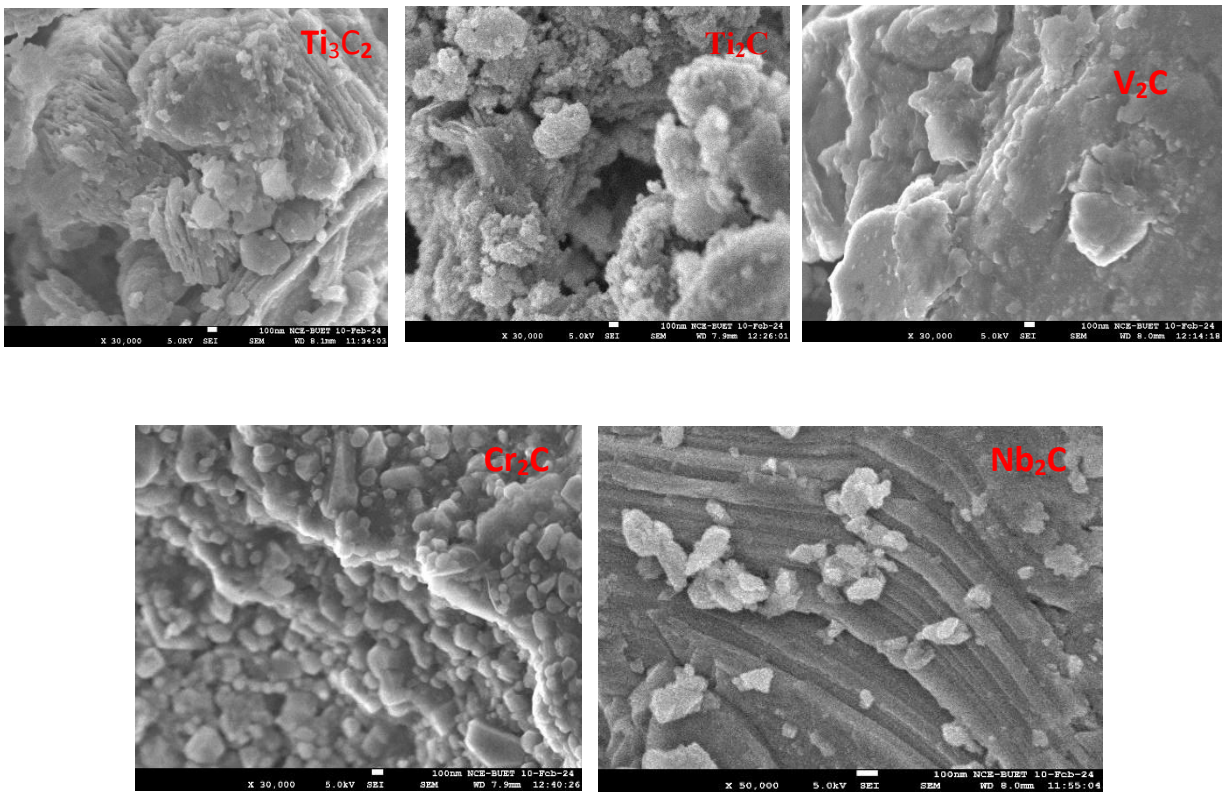


Figure 4.4: SEM images of various MXenes materials synthesized by etching technique.

4.3 FUNCTIONAL GROUP ANALYSIS BY FTIR

Fourier Transform Infrared (FTIR) analysis looks at how compounds interact with infrared light to identify and understand substances. In essence, it measures the amount of infrared light absorbed by various chemical bonds at various wavelengths. Figure 4.5 displays the room temperature FTIR spectra of the MXenes Ti_3C_2, TiC, V_2C, Cr_2C, and Nb_2C under study. Several characteristic peaks of the samples are seen between 800 and 4000 cm^{-1}. The modes of the O-H vibration peak between 3200 cm^{-1} and 4000 cm^{-1}. The O-H bond is found in all samples of Ti_3C_2 between 3600 and 3750 cm^{-1}, while it is moved to 3300 cm^{-1} in Ti_3C. Every sample that falls between 1550 and 1630 cm^{-1} has a C-O bond. In

addition, the C-F bond, which results from the use of LiF during the etching process, is present in all samples except Ti_3C_2 in the 950–1150 cm^{-1} range. Consistent with the literature, additional bonds are also seen at different wavenumbers. Therefore, the FTIR spectra confirmed the materials' purity in conjunction with XRD investigation.

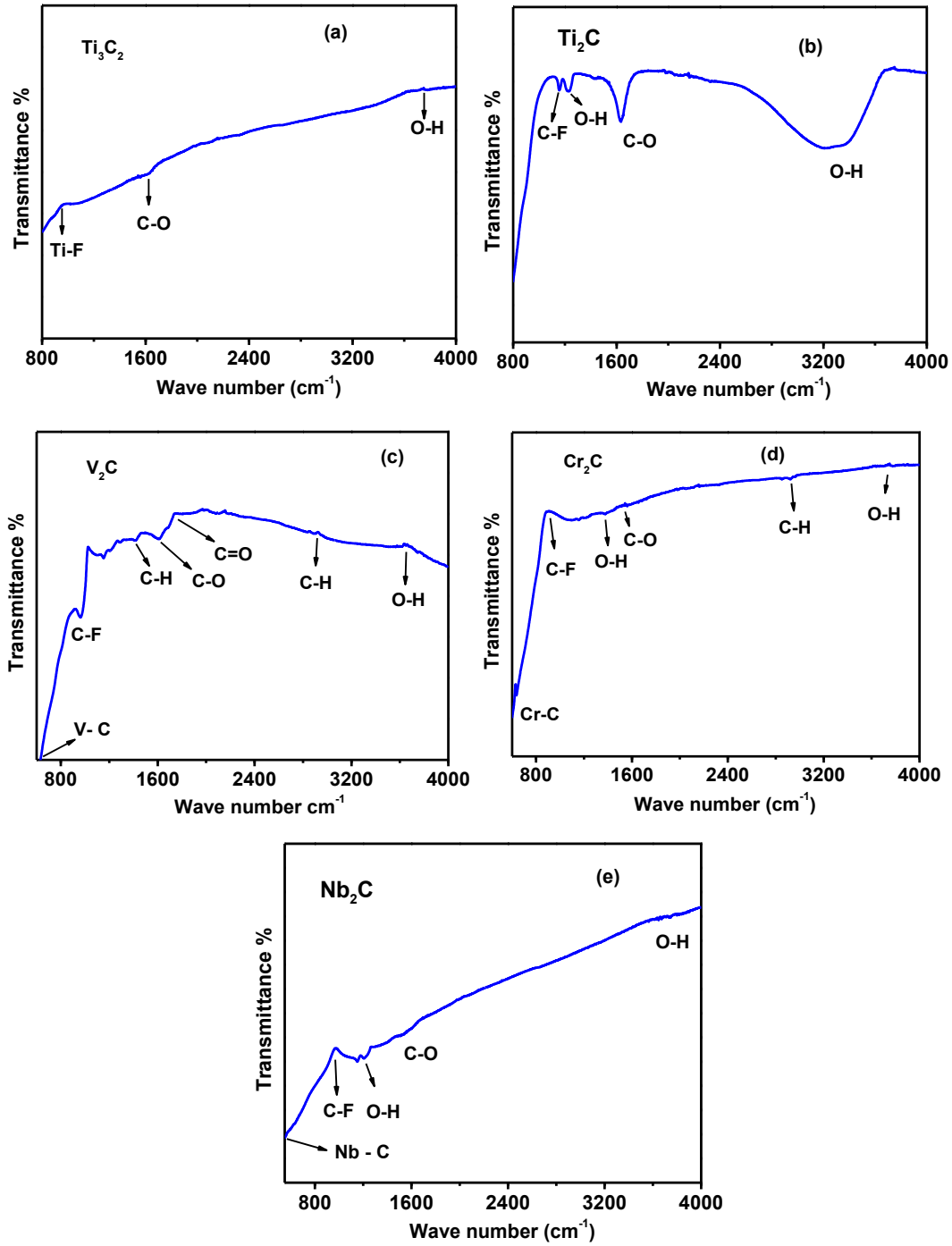


Figure 4.5: FTIR images of various MXenes materials.

4.4 PHOTOCATALYTIC PERFORMANCE

4.4.1 BAND GAP

According to reports, the band gap of MXenes materials ranges from 0.92 eV to 1.75 eV [62,63]. The bandgap of the MXenes powder samples was determined using the Kubelka–Munk (K–M) technique. The predicted bandgap of the samples based on room temperature UV-vis diffuse reflectance spectroscopy (DRS) data is shown in the figure 8. The K-M equation relates reflectance (R) to the K-M function F(R), as per the following equation.

$$F(R) = \frac{(1-R)^2}{2R}, \qquad (5)$$

Plotting the $[F(R)*h\upsilon]^2$ vs *energy* graph, however, yields E_g since F(R) is exactly proportional to the coefficient of absorption, α. However, the following equation provides the link between

$$F \propto \alpha$$

$$F(R)*h\upsilon = A\,(h\upsilon - E_g)^n, \qquad (6)$$

The photon's energy is denoted by hυ, Planck's constant by h, the proportionality constant by A, and the required bandgap energy by E_g. Indirect and direct optical band gaps are represented by the values of n as ½ and 2, respectively. In this case, we calculated the direct bandgap of all generated samples using n=2. The optical bandgap's directness or indirectness is determined by the value of n in this equation. The band gap value falls between 1.76 and 1.81 eV. The obtained bandgap ranges agree with those that have been published [64]. This band gap demonstrates that MXenes materials may be used in a variety of fields, including EMI shielding, Li-ion batteries, and photocatalysis.

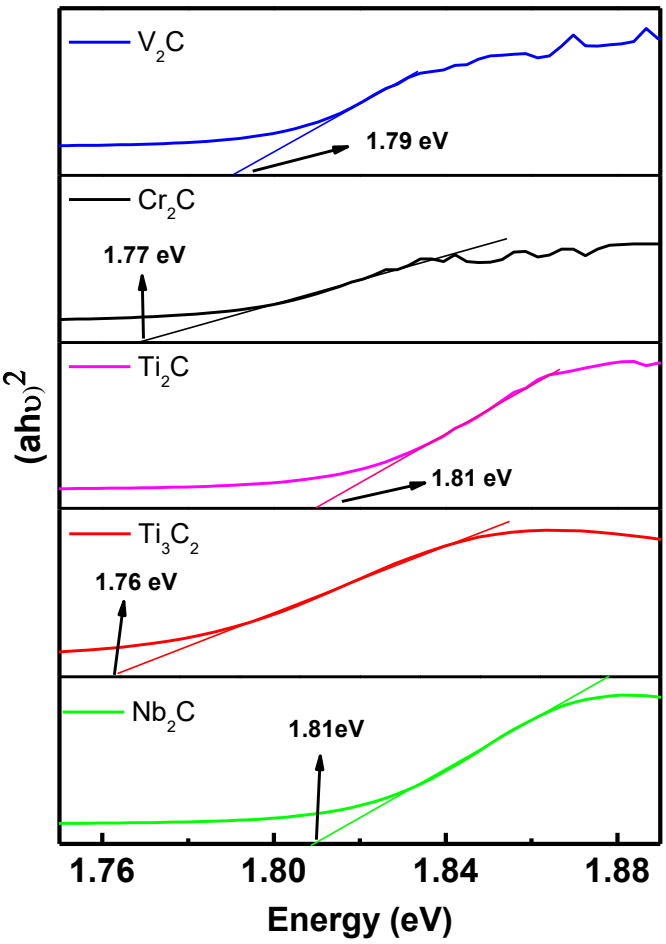
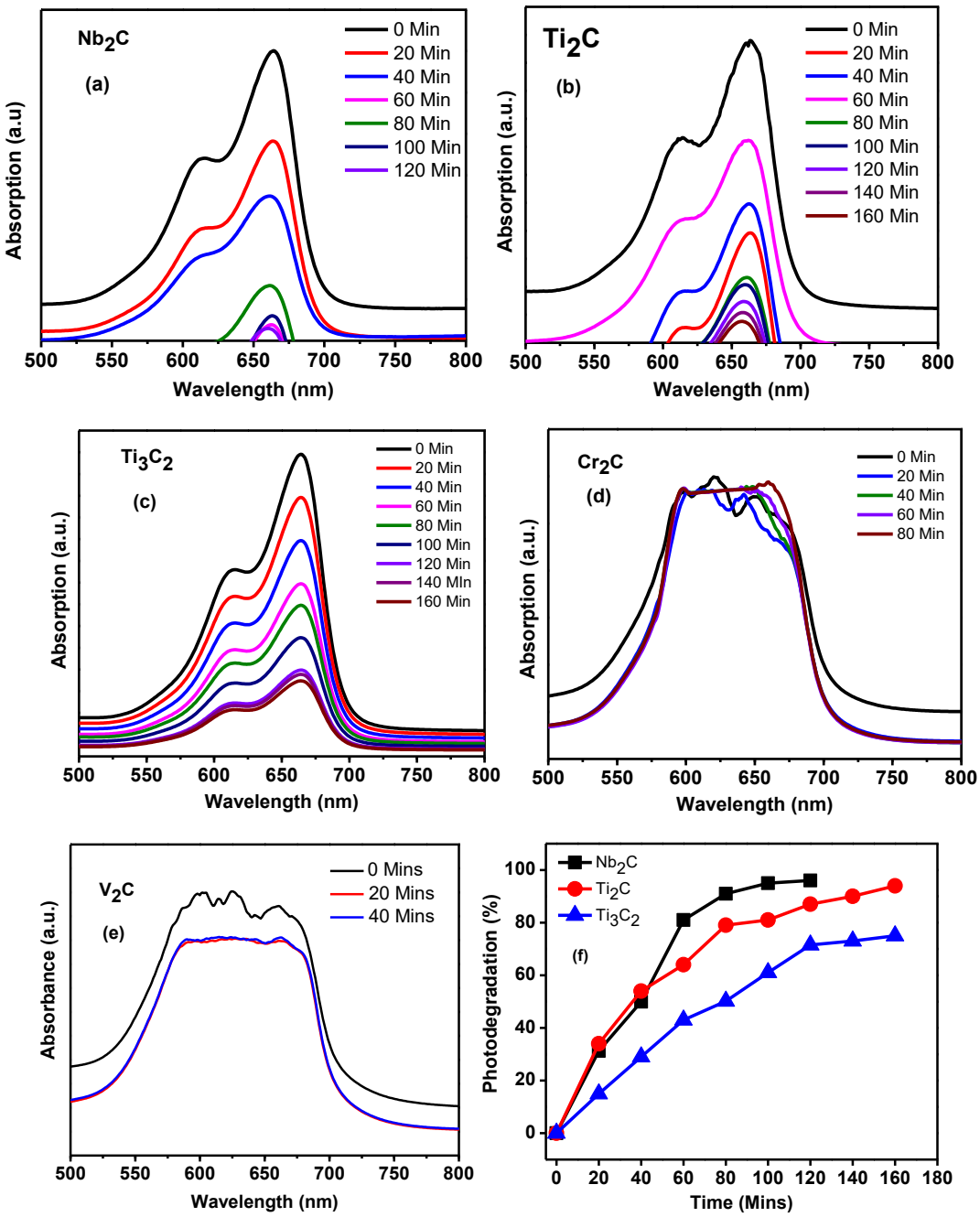


Figure 4.6: Tauc's plot for measuring the band gap of MXenes materials.

4.4.2 PHOTOCATALYTIC ACTIVITY

Methylene blue (MB) dye's photocatalytic degradation activity has been examined utilizing five samples that were all manufactured under identical conditions Photocatalysis was conducted for up to 180 minutes in an aquatic medium using deionized water under visible light (LED) irradiation. Fig. 4.7 displays the time variable UV-vis absorption spectra of MXenes materials. Fig. 4.7f displays the C/C_0 curve for MB degradation in both samples, indicating the concentration of MB at adsorption equilibrium and the remaining non-degraded dye after irradiation. The following formula is used to measure the degree of deterioration efficiency:

$$\text{Degradation (\%)} = \left(1 - \frac{C}{C_o}\right) \times 100\%, \qquad (7)$$



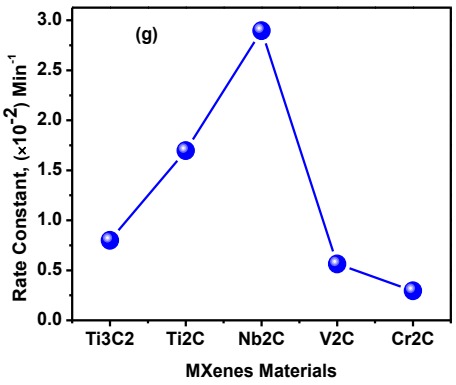


Figure 4.7: (a-e) Wavelength dependent absorption curves of the sitdied MXenes. (f) photodegradation efficiency of various MXenes 2D materials. (g) time constant of different MXenes materials.

As seen in Fig. 4.7 f, the data indicates that the MXenes samples had exceptional photodegradation efficiency. To be more precise, Nb_2C obtains a degradation efficiency of 96% after 120 minutes of irradiation, whereas Ti_2C reaches 94% after just 160 minutes. When compared to TiC and Nb_2C materials, Ti_3C_2 exhibits somewhat poorer efficiency, achieving 75% deterioration after 160 minutes. Furthermore, during 40 minutes of irradiation, two of the MXenes samples, Cr_2C and V_2C, show a much-reduced performance loss (20%). As was previously discussed, the agglomerated state of the Cr_2C MXenes in the SEM pictures may be the cause of the reduced photodegradation effectiveness. The photodegradation efficiency in the instance of V_2C is likewise found to be very low; measurements are repeated, but the findings are comparable. The process or cause of this is still unknown.

Figure 4.7 g shows the rate constant of the MXenes photodegradation. It's noteworthy that V_2C and Cr_2C have lower rate constants than Nb_2C, Ti_2C, and Ti_3C_2. In order to improve the performance of photocatalysts like MXenes, recombination must be minimized because it is in fact harmful to photodegradation efficiency. In order to facilitate charge separation and reduce recombination, surface functionalization—such as the addition of oxygen, fluorine, or hydroxyl groups—can enhance the production of reactive oxygen species (ROS) or assist establish active spots for electron trapping. Fluorine's (F)

surface modification of MXenes enhances degradation efficiency by creating sites for hydroxyl radicals and superoxide anions, which break down contaminants. Surface alterations, flaws, and active sites are absent in V_2C and Cr_2C, which is harmful to photodegradation in photocatalytic processes (as seen in SEM images, Fig. 4.4). Ti_2C and Nb_2C are especially interesting candidates for efficient photodegradation processes based on the degradation and rate constant.

4.5 SHIELDING ANALYSIS BY MCNP

The first step is to design our geometry of the HPGe detector. Geometry of the detector is shown as in Figure 4.8. Normally the radius of the point source is 2.5 cm as a result we consider our sample size of 2.5 cm, here the thickness of the source is 1 mm. We consider the distance between source and sample is 2 cm, here our target is to take the distance as much as lower. Again, the distance between MXene and detector is 3 cm.

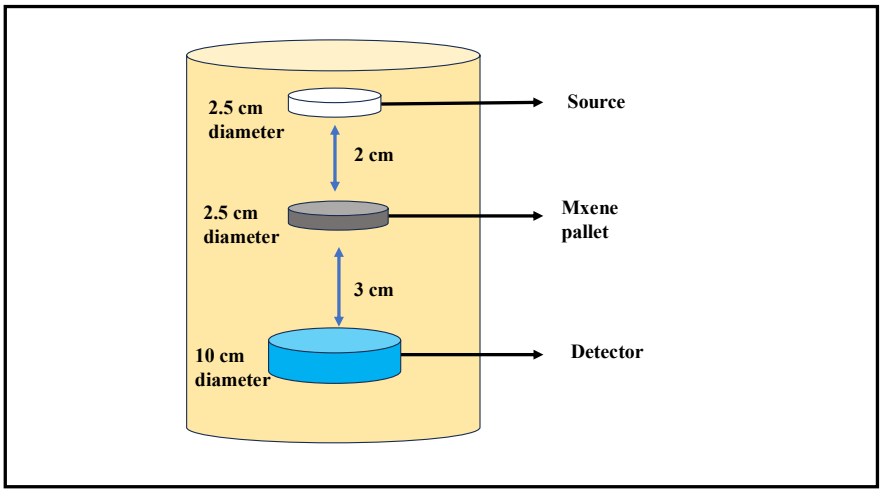


Figure 4.8: Geometry of experimental set up.

The theoretical results are given in the table below:

Table-2: Measurement of dose rate shielded by MXene materials using MCNP code.

MXenes materials	Density (g/cm^3)	Thickness (cm)	Radiation Type	Energy (MeV)	Initial Dose Rate (mSv/h)	Shielded Dose Rate *(mSv/h)*	Attenuation Coefficient (cm^{-1})	Relative Error
$Ti_3C_2T_x$	4.50	0.5	^{137}Cs	0.662	33.0	19.6	1.20	1.5
Nb_2CT_x	5.50					12.7	1.40	1.4
$TiCT_x$	4.40					10.7	1.25	1.5
V_2CT_x	5.10					9.6	2.0	1.4
Cr_2CT_x	5.30					8.8	2.5	1.6

The table presents detailed information on the radiation shielding performance of several MXenes materials, namely $Ti_3C_2T_x$, Nb_2C_x, Ti_2C_x, V_2C_x, and Cr_2C_x, under gamma radiation exposure. Each material sample used for this situdy had a consistent thickness of 0.5 cm. The density of these materials varied slightly, ranging from 4.40 g/cm^3 to 5.50 g/cm^3. The radiation source for all experiments was a cesium-137 (^{137}Cs) isotope, which emits gamma rays with a photon energy of 0.662 MeV. This uniform setup ensures that the comparative shielding performance across the different MXenes materials can be fairly evaluated.

Initially, before any shielding was applied, the gamma radiation dose rate was recorded at 33.0 mSv/h for all samples. After passing through the MXene materials, the shielded dose rates decreased significantly but varied depending on the type of material used. $Ti_3C_2T_x$ reduced the dose rate to 19.6 mSv/h, while Nb_2C_x provided a stronger reduction to 12.7 mSv/h. Ti_2C_x further lowered the dose to 10.7 mSv/h, and V_2C_x achieved a reduction down to 9.6 mSv/h. The best performance was observed in Cr_2C_x, which reduced the dose rate to 8.8 mSv/h.

These reductions clearly show that the shielding capability improves with certain material properties, particularly with higher material density.

The linear attenuation coefficient (μ), an important measure of a material's ability to attenuate radiation, was also calculated for each MXene. The attenuation coefficient values ranged from 1.20 cm^{-1} for $Ti_3C_2T_x$ to 2.50 cm^{-1} for Cr_2C_x. A higher attenuation coefficient indicates a greater ability to absorb or scatter radiation, thus providing better shielding effectiveness. Cr_2C_x, with the highest attenuation coefficient among the tested materials, demonstrated the most promising shielding performance, correlating well with its relatively high density of 5.30 g/cm^3.

Additionally, the relative errors associated with the experimental measurements were recorded for each material and found to range between 1.4% and 1.6%. These low error percentages suggest that the results are reliable and that the experimental methodology was consistent and accurate across all the tested samples.

Overall, the data highlight a strong relationship between the density of MXenes and their radiation shielding effectiveness. Denser MXenes tend to offer better protection against gamma radiation, as evidenced by their lower shielded dose rates and higher attenuation coefficients. This study underscores the potential of MXenes as effective lightweight radiation shielding materials, suitable for various applications where high-performance, thin, and efficient shields are necessary, such as in medical radiation protection, nuclear industries, and aerospace sectors.

Additionally, the chemical composition of the material affects its interaction with radiation. Materials with heavier atomic elements tend to have higher atomic numbers (Z), and gamma ray attenuation generally increases with atomic

number. Thus, MXenes with heavier or more tightly packed atoms are better at shielding.

In short, the shielded dose rate varies because materials with higher densities and higher atomic numbers interact more strongly with gamma radiation, reducing the amount of radiation that passes through.

4.6 CREDIBLE MECHANISM OF DEGRADATION AND REVIEW REPORT

Figure 4.9 shows the potential pathway of pollutant breakdown utilizing the catalyst and dye MB. Photons are emitted from the valence band (VB) of the catalyst surface, moving to the conduction band (CB). Recombination can occur due to the electron and hole themselves or surface charges. We measure the effectiveness of photocatalysis by precisely regulating the recombination rate. Because of the surface functional groups (such as -OH, -O, and -F), the formation of vacancies for titanium (niobium) and oxygen between the atoms results in a variety of defects and adds additional energy states to the bandgap, which regulates recombination. Researchers are studying energy states at trapping sites to expedite the breakdown process, prolong the lifetime of photo-excitons, and prevent electron-hole recombination.

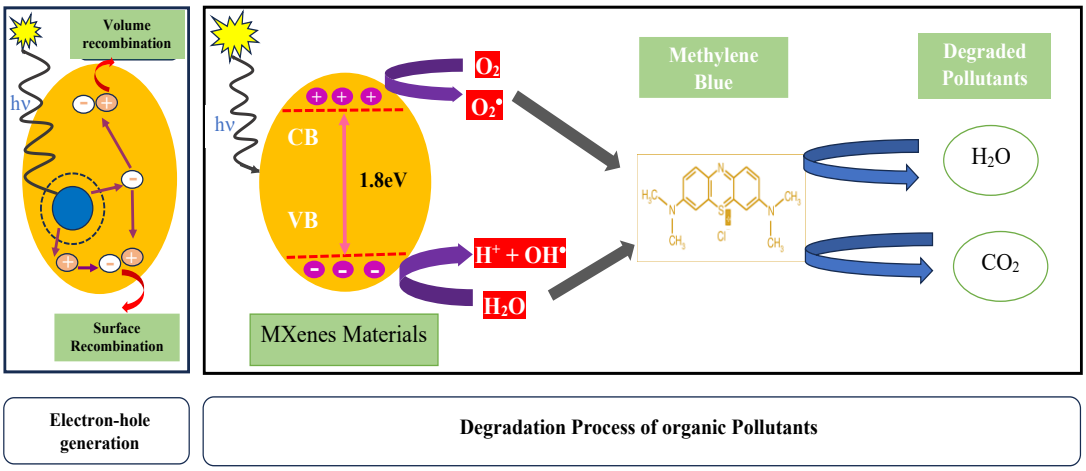


Figure 4.9: Schematic diagram of photocatalytic process of MXenes materials.

Now table-3 presents a comparative analysis of several MXene-derived catalysts in the degradation of methylene blue (MB**)** under light exposure, highlighting both previously reported materials and newly tested ones in this situdy.

Among the earlier situdies, **Nb_2CTx** and its modified form **Nb_2CTx-12**, used at 25 mg with an MB concentration of 18 mg/L for 180 minutes, achieved degradation efficiencies of 15.3% and 26.9%, with rate constants of 0.13 and 0.21×10^{-2} min^{-1}, respectively. **V_2C**, used at a higher amount (50 mg) and lower MB concentration (10 mg/L) for 120 minutes, achieved only 13% degradation with a similar rate constant of 0.12×10^{-2} min^{-1}. **Ti_3C_2**, used at 35 mg and a much higher MB concentration (30 mg/L) for 40 minutes, also resulted in a modest 14% degradation with a rate constant of 0.12×10^{-2} min^{-1}.

In contrast, the materials tested in this work show significantly enhanced photocatalytic performance under comparable or even milder conditions. Nb_2C, used at only 10 mg with a low MB concentration of 3.55 mg/L for 120 minutes, achieved a remarkable 96% degradation efficiency with a rate constant of 2.89×10^{-2} min^{-1}—the highest among all entries. Similarly, TiC, under similar conditions for 160 minutes, showed an excellent 94% degradation and a rate constant of 0.17×10^{-2} min^{-1}. Ti_3C_2, also tested in this work with 10 mg of catalyst, resulted in a 75% degradation efficiency and a rate constant of 0.79×10^{-2} min^{-1}—much higher than its previously reported counterpart.

Overall, the results clearly demonstrate that Nb_2C and TiC, as tested in this study, outperform other MXene-based materials in photocatalytic activity. Their superior degradation efficiency and significantly higher rate constants suggest excellent potential for environmental remediation applications, particularly in the photodegradation of organic dyes like methylene blue.

Table 3: Comparative summary of the available MXenes materials and obtained results for the photodegradation efficiency of MB.

MXenes materials	Catalyst amount (mg)	MB concentration	Light Source (Mins)	Degradation efficiency	Rate constant (min^{-1}) x 10^{-2}	Reference
Nb_2CT_x	25	18 mg/L	180	15.3%	0.13	[47]
Nb_2CT_{x-12}	25	18 mg/L	180	26.9%	0.21	[47]
V_2C	50	10 mg/L	120	13%	0.12	[56]
Ti_3C_2	35	30 mg/L	40	14%	0.12	[65]
TiC	10	3.55 mg/L	160	94%	0.17	This Work
Nb_2C	10	3.55 mg/L	120	96%	2.89	This Work
Ti_3C_2	10	3.55 mg/L	160	75%	0.79	This Work

Also, table 3 contrasts our findings with the published MXenes photocatalytic performance. Degradation efficiency and number of measurement parameters, including energy source, catalyst concentration, pollutant concentration, and degradation duration, influence degradation efficiency. Based on the stated MXenes photodegradation efficiency, a higher concentration of catalyst and contaminants leads to a lower degradation percentage as illustrated in Table 3. The best degrading performance has been achieved among all published MXenes samples by using a lower MB concentration compared to reported MXenes system. The rate constant calculates, at first, the value of C/C_0 calculated. The Beer-Lambert law states that the concentration of an absorbent is directly proportional to its absorbance. Therefore: $C/C_0 = A/A_0$. Then taking ln of C/C_0.

After plotting the $\ln(C/C_0)$ vs time that makes a line. The rate constant is being calculated using the slope of line [29,66]. Nevertheless, out of all the MXenes systems described, our determined degradation rate constants for Nb_2C (2.89 min^{-1}) and Ti_3C_2 (0.79 min^{-1}) are the highest. It is clear that the utmost options for photodegradation in the MXenes system are of Nb_2C, Ti_2C, and Ti_3C_2.

Chapter 5: CONCLUSIONS

5.1 GENERAL

MXenes, as a class of two-dimensional transition metal carbides, exhibit significant potential for photocatalytic applications due to their high surface area, tunable electrical properties, and ability to generate reactive species. This work successfully synthesized multiple MXenes (Nb_2C, Ti_2C, Ti_3C_2, Cr_2C, and V_2C) using an in-situ HF etching approach, which is safer than conventional HF-based methods. The prepared MXenes demonstrated promising structural stability, suitable morphology, and effective optical properties, indicating their suitability for environmental remediation.

5.2 KEY FINDINGS

MXenes were synthesized from MAX phase precursors using LiF + HCl, avoiding the direct use of hazardous HF while maintaining high material quality. Photodegradation efficiencies achieved were up to 96% for Nb_2C, 94% for Ti_2C, and 75% for Ti_3C_2 within respective reaction times. Kinetic analysis revealed high-rate constants, particularly for Nb_2C (2.89 min^{-1}), Ti_3C_2 (0.79 min^{-1}), and Ti_2C (0.17 min^{-1}), highlighting their superior catalytic activity. SEM analyses confirmed increased interlayer gaps and larger surface areas, which enhanced photocatalytic performance.

5.3 PRACTICAL IMPLICATION

The results suggest that Nb_2C, Ti_2C, and Ti_3C_2 MXenes can serve as efficient and rapid catalysts for treating environmental pollutants, particularly organic dyes in wastewater. Their high efficiency, coupled with a safer synthesis process, makes them suitable candidates for future scalable applications in industrial water purification and environmental remediation technologies.

5.4 SUGGESTIONS FOR FURTHER RESEARCH WORK

Investigate transition metal or rare-earth element doping to further tune the bandgap and improve photodegradation efficiency. Explore large-scale synthesis techniques to enable industrial implementation while maintaining safety and cost-effectiveness. Study the long-term stability and reusability of MXene-based catalysts in real wastewater conditions. Examine composite or hybrid MXene structures to enhance multifunctionality (e.g., combining photocatalysis with antibacterial or EMI shielding properties).

BIBLIOGRAPHY

[1] M. Naguib, M. Kurtoglu, V. Presser, J. Lu, J. Niu, M. Heon, L. Hultman, Y. Gogotsi, M.W. Barsoum, Two-dimensional nanocrystals produced by exfoliation of Ti 3AlC 2, Advanced Materials 23 (2011) 4248–4253. https://doi.org/10.1002/adma.201102306.

[2] D. Dhamodharan, V. Dhinakaran, H.-S. Byun, MXenes: An emerging 2D material, Carbon N Y 192 (2022) 366–383. https://doi.org/https://doi.org/10.1016/j.carbon.2022.03.004.

[3] J. Yang, M. Naguib, M. Ghidiu, L.M. Pan, J. Gu, J. Nanda, J. Halim, Y. Gogotsi, M.W. Barsoum, Two-Dimensional Nb-Based M4C3 Solid Solutions (MXenes), Journal of the American Ceramic Society 99 (2016). https://doi.org/10.1111/jace.13922.

[4] Md.M. Uddin, M.H. Kabir, Md.A. Ali, Md.M. Hossain, M.U. Khandaker, S. Mandal, A. Arifutzzaman, D. Jana, Graphene-like emerging 2D materials: recent progress challenges and future outlook, RSC Adv. 13 (2023) 33336–33375. https://doi.org/10.1039/D3RA04456D.

[5] R.V. And, G. Madras, Environmental remediation by photocatalysis, n.d.

[6] M. Mishra, D.-M. Chun, α-Fe 2 O 3 as a photocatalytic material: A review, Appl Catal A Gen 498 (2015) 126–141. https://doi.org/10.1016/j.apcata.2015.03.023.

[7] R. Vinu, and Giridhar Madras, Environmental remediation by photocatalysis, (n.d.).

[8] Y. Lu, H. Zhang, D. Fan, Z. Chen, X. Yang, Coupling solar-driven photothermal effect into photocatalysis for sustainable water treatment, J Hazard Mater 423 (2022) 127128. https://doi.org/10.1016/j.jhazmat.2021.127128.

[9] R. Abazari, S. Sanati, L.A. Saghatforoush, Non-aggregated divanadium pentoxide nanoparticles: A one-step facile synthesis. Morphological, structural, compositional, optical properties and photocatalytic activities, Chemical Engineering Journal 236 (2014) 82–90. https://doi.org/10.1016/j.cej.2013.09.056.

[10] M.M. Khan, S.F. Adil, A. Al-Mayouf, Metal oxides as photocatalysts, Journal of Saudi Chemical Society 19 (2015) 462–464. https://doi.org/10.1016/j.jscs.2015.04.003.

[11] A.B. Djurišić, Y.H. Leung, A.M.C. Ng, Strategies for improving the efficiency of semiconductor metal oxide photocatalysis, Mater Horiz 1 (2014) 400–410. https://doi.org/10.1039/C4MH00031E.

[12] H. Wang, L. Zhang, Z. Chen, J. Hu, S. Li, Z. Wang, J. Liu, X. Wang, Semiconductor heterojunction photocatalysts: Design, construction, and photocatalytic performances, Chem Soc Rev 43 (2014) 5234–5244. https://doi.org/10.1039/C4CS00126E.

[13] M. Serda, F.G. Becker, M. Cleary, R.M. Team, H. Holtermann, D. The, N. Agenda, P. Science, S.K. Sk, R. Hinnebusch, R.H. A, I. Rabinovich, Y. Olmert, D.Q.G.L.Q. Uld, W.K.H.U. Ri, V. Lq, W.K.H. Frxqwu, E. Zklfk, L. V Edvhg, R.Q. Wkh, F.G. Becker, N. Aboueldahab, R. Khalaf, L.R. De Elvira, T. Zintl, R. Hinnebusch, M. Karimi, S.M.M. Shafaee, D.O. 'driscoll, S. Watts, J. Kavanagh, B. Frederick, T. Norlen, A. O'Mahony, P. Voorhies, T. Szayna, N. Spalding, M.O. Jackson, M. Morelli, B. Satpathy, B. Muniapan, M. Dass, P. Katsamunska, Y. Pamuk, A. Stahn, E. Commission, T.E.D. Piccone, Mr.K. Annan, S. Djankov, M. Reynal-Querol, M. Couttenier, R. Soubeyran, P. Vym, E. Prague, W. Bank, C. Bodea, N. Sambanis, A. Florea, A. Florea, M. Karimi, S.M.M. Shafaee, N. Spalding, N. Sambanis, فاطمی .ح, Synteza i aktywność biologiczna nowych analogów tiosemikarbazonowych chelatorów żelaza, Uniwersytet Śląski 7 (2013) 343–354. https://doi.org/10.2/JQUERY.MIN.JS.

[14] E. Pelizzetti, C. Minero, Metal Oxides as Photocatalysts for Environmental Detoxification, Comments on Inorganic Chemistry 15 (1994) 297–337. https://doi.org/10.1080/02603599408035846.

[15] J. Kang, W. Sun, Y. Hu, Z. Gao, R. Liu, Q. Zhang, H. Liu, X. Meng, The utilization of waste by-products for removing silicate from mineral processing wastewater via chemical precipitation, Water Res 125 (2017) 318–324. https://doi.org/10.1016/j.watres.2017.08.047.

[16] J. Wang, L. Chu, Biological nitrate removal from water and wastewater by solid-phase denitrification process, Biotechnol Adv 34 (2016) 1103–1112. https://doi.org/10.1016/j.biotechadv.2016.07.001.

[17] M.~ E.R.N. A, Use of Solvent Extraction for the Removal of Heavy Metals from Liquid Wastes (n.d.).

[18] strathmann1981, (n.d.).

[19] J. Kim, Y. Chung, D. Shin, M. Kim, Y. Lee, Y. Lim, D. Lee, Chlorination by-products in surface water treatment process, Desalination 151 (2003) 1–9. https://doi.org/https://doi.org/10.1016/S0011-9164(02)00967-0.

[20] S.N. Malik, P.C. Ghosh, A.N. Vaidya, S.N. Mudliar, Hybrid ozonation process for industrial wastewater treatment: Principles and applications: A review, Journal of Water Process Engineering 35 (2020). https://doi.org/10.1016/j.jwpe.2020.101193.

[21] J.A. Ritter, Removal of Mercury from Waste Water: Large Scale Performance of an Ion Exchange Process, Wat. Sci. Tech 25 (1992) 165–172.

[22] G.B.S.S. Kirill Fedorov Manoj P. Rayaroth, Degradation of 1,4-dioxane by sono-activated persulfates for water and wastewater treatment applications, Water Resour Ind 28 (2022) 100183.

[23] Y.M. Hunge, A.A. Yadav, S. Liu, V.L. Mathe, Sonochemical synthesis of CZTS photocatalyst for photocatalytic degradation of phthalic acid, Ultrason Sonochem 56 (2019) 284–289. https://doi.org/https://doi.org/10.1016/j.ultsonch.2019.04.003.

[24] Y.M. Hunge, A.A. Yadav, S. Khan, K. Takagi, N. Suzuki, K. Teshima, C. Terashima, A. Fujishima, Photocatalytic degradation of bisphenol A using titanium dioxide nanodiamond composites under UV light illumination, J Colloid Interface Sci 582 (2021) 1058–1066. https://doi.org/https://doi.org/10.1016/j.jcis.2020.08.102.

[25] Y.M. Hunge, A.A. Yadav, S.B. Kulkarni, V.L. Mathe, A multifunctional ZnO thin film-based devices for photoelectron catalytic degradation of terephthalic acid and CO2 gas sensing applications, Sens Actuators B Chem 274 (2018) 1–9. https://doi.org/https://doi.org/10.1016/j.snb.2018.07.117.

[26] W.-J. Ong, L.-L. Tan, S.-P. Chai, S.-T. Yong, A.R. Mohamed, Highly reactive {001} facets of TiO2-based composites: synthesis, formation mechanism and characterization, Nanoscale 6 (2014) 1946–2008. https://doi.org/10.1039/C3NR04655A.

[27] P.M. Álvarez, J. Jaramillo, F. López-Piñero, P.K. Plucinski, Preparation and characterization of magnetic TiO2 nanoparticles and their utilization for the degradation of emerging pollutants in water, Appl Catal B 100 (2010) 338–345. https://doi.org/https://doi.org/10.1016/j.apcatb.2010.08.010.

[28] M.A. Jalil, M.N.I. Khan, S.K. Mandal, F.-U.-Z. Chowdhury, M.M. Hossain, D. Jana, M.S. Alam, M.M. Uddin, Impact of reaction temperatures on the particle size of V2O5 synthesized by facile hydrothermal technique and photocatalytic efficacy in dye degradation, AIP Adv 13 (2023) 15010. https://doi.org/10.1063/5.0125200.

[29] M.H. Kabir, M.Z. Hossain, M.A. Jalil, S. Ghosh, M.M. Hossain, M.A. Ali, M.U. Khandaker, D. Jana, M.M. Rahman, M.K. Hossain, J. Chowdhury, M. Kazi, M.M. Uddin, The efficacy of rare-earth doped V2O5 photocatalyst for removal of pollutants from industrial wastewater, Opt Mater (Amst) 147 (2024) 114724. https://doi.org/https://doi.org/10.1016/j.optmat.2023.114724.

[30] Z. Li, Y. Wu, 2D Early Transition Metal Carbides (MXenes) for Catalysis, Small 15 (2019) 1804736. https://doi.org/https://doi.org/10.1002/smll.201804736.

[31] I.M. Chirica, A.G. Mirea, Ş. Neaţu, M. Florea, M.W. Barsoum, F. Neaţu, Applications of MAX phases and MXenes as catalysts, J. Mater. Chem. A 9 (2021) 19589–19612. https://doi.org/10.1039/D1TA04097A.

[32] N.H. Ahmad Junaidi, W.Y. Wong, K.S. Loh, S. Rahman, W.R.W. Daud, A comprehensive review of MXenes as catalyst supports for the oxygen reduction reaction in fuel cells, Int J Energy Res 45 (2021) 15760–15782. https://doi.org/https://doi.org/10.1002/er.6899.

[33] G. Li, N. Li, S. Peng, B. He, J. Wang, Y. Du, W. Zhang, K. Han, F. Dang, Highly Efficient Nb2C MXene Cathode Catalyst with Uniform O-Terminated Surface for Lithium–Oxygen Batteries, Adv Energy Mater 11 (2021) 2002721. https://doi.org/https://doi.org/10.1002/aenm.202002721.

[34] D. Ponnalagar, D.-R. Hang, S.E. Islam, C.-T. Liang, M.M.C. Chou, Recent progress in two-dimensional Nb_2C MXene for applications in

energy storage and conversion, Mater Des 231 (2023) 112046. https://doi.org/https://doi.org/10.1016/j.matdes.2023.112046.

[35] A. Shahzad, K. Rasool, M. Nawaz, W. Miran, J. Jang, M. Moztahida, K.A. Mahmoud, D.S. Lee, Hetero structural TiO_2/Ti_3C_2Tx (MXene) for photocatalytic degradation of antiepileptic drug carbamazepine, Chemical Engineering Journal 349 (2018) 748–755. https://doi.org/10.1016/j.cej.2018.05.148.

[36] A. Shahzad, K. Rasool, W. Miran, M. Nawaz, J. Jang, K.A. Mahmoud, D.S. Lee, Mercuric ion capturing by recoverable titanium carbide magnetic nanocomposite, J Hazard Mater 344 (2018) 811–818. https://doi.org/https://doi.org/10.1016/j.jhazmat.2017.11.026.

[37] C.J. Zhang, S. Pinilla, N. McEvoy, C.P. Cullen, B. Anasori, E. Long, S.-H. Park, A. Seral-Ascaso, A. Shmeliov, D. Krishnan, C. Morant, X. Liu, G.S. Duesberg, Y. Gogotsi, V. Nicolosi, Oxidation Stability of Colloidal Two-Dimensional Titanium Carbides (MXenes), Chemistry of Materials 29 (2017) 4848–4856. https://doi.org/10.1021/acs.chemmater.7b00745.

[38] Z. Othman, A. Sinopoli, H.R. Mackey, K.A. Mahmoud, Efficient Photocatalytic Degradation of Organic Dyes by $AgNPs/TiO_2/Ti_3C_2Tx$ MXene Composites under UV and Solar Light, ACS Omega 6 (2021) 33325–33338. https://doi.org/10.1021/acsomega.1c03189.

[39] A. Iqbal, J. Kwon, M.K. Kim, C.M. Koo, MXenes for electromagnetic interference shielding: Experimental and theoretical perspectives, Mater Today Adv 9 (2021). https://doi.org/10.1016/j.mtadv.2020.100124.

[40] R. Verma, P. Thakur, A. Chauhan, R. Jasrotia, A. Thakur, A review on MXene and its' composites for electromagnetic interference (EMI) shielding applications, Carbon N Y 208 (2023) 170–190. https://doi.org/https://doi.org/10.1016/j.carbon.2023.03.050.

[41] M. Han, C.E. Shuck, R. Rakhmanov, D. Parchment, B. Anasori, C.M. Koo, G. Friedman, Y. Gogotsi, Beyond Ti3C2Tx: MXenes for Electromagnetic Interference Shielding, ACS Nano 14 (2020) 5008–5016. https://doi.org/10.1021/acsnano.0c01312.

[42] T. Cui, F. Wang, L. Bing, R. Wang, Z. Ma, Q. Jia, Monte Carlo simulation and optimization of neutron ray shielding performance

of related materials, Nuclear Engineering and Technology 56 (2024) 3545–3552. https://doi.org/https://doi.org/10.1016/j.net.2024.04.002.

[43] S. Bilici, M. Kamislioglu, E.E. Altunsoy Guclu, A Monte Carlo simulation study on the evaluation of radiation protection properties of spectacle lens materials, The European Physical Journal Plus 138 (2023) 80. https://doi.org/10.1140/epjp/s13360-022-03579-6.

[44] I.A. Alsafari, S. Munir, S. Zulfiqar, M.S. Saif, M.F. Warsi, M. Shahid, Synthesis, characterization, photocatalytic and antibacterial properties of copper Ferrite/MXene (CuFe2O4/Ti3C2) nanohybrids, Ceram Int 47 (2021) 28874–28883. https://doi.org/10.1016/j.ceramint.2021.07.048.

[45] O. Mashtalir, K.M. Cook, V.N. Mochalin, M. Crowe, M.W. Barsoum, Y. Gogotsi, Dye adsorption and decomposition on two-dimensional titanium carbide in aqueous media, J. Mater. Chem. A 2 (2014) 14334–14338. https://doi.org/10.1039/C4TA02638A.

[46] T. Wojciechowski, A. Wojciechowska, G. Matyszczak, M. Wrzecionek, A. Olszyna, A. Peter, A. Mihaly-Cozmuta, N. Camelia, L. Mihaly Cozmuta, S. Podsiadło, D. Basiak, W. Ziemkowska, A. Jastrzębska, Ti2C MXene Modified with Ceramic Oxide and Noble Metal Nanoparticles: Synthesis, Morphostructural Properties, and High Photocatalytic Activity, Inorg Chem 58 (2019). https://doi.org/10.1021/acs.inorgchem.9b01015.

[47] C. Cui, R. Guo, E. Ren, H. Xiao, X. Lai, Q. Qin, S. Jiang, H. Shen, M. Zhou, W. Qin, Facile hydrothermal synthesis of rod-like Nb_2O_5/Nb_2CTx composites for visible-light driven photocatalytic degradation of organic pollutants, Environ Res 193 (2021). https://doi.org/10.1016/j.envres.2020.110587.

[48] R. Xu, G. Wei, Z. Xie, S. Diao, J. Wen, T. Tang, L. Jiang, M. Li, G. Hu, V_2C MXene-modified g-C_3N_4 for enhanced visible-light photocatalytic activity, n.d.

[49] Z. Othman, A. Sinopoli, H.R. Mackey, K.A. Mahmoud, Efficient Photocatalytic Degradation of Organic Dyes by AgNPs/TiO_2/Ti_3C_2Tx MXene Composites under UV and Solar Light, ACS Omega 6 (2021) 33325–33338. https://doi.org/10.1021/acsomega.1c03189.

[50] Z. Kalaycıoğlu, B. Özuğur Uysal, Ö. Pekcan, F.B. Erim, Efficient Photocatalytic Degradation of Methylene Blue Dye from Aqueous

Solution with Cerium Oxide Nanoparticles and Graphene Oxide-Doped Polyacrylamide, ACS Omega 8 (2023) 13004–13015. https://doi.org/10.1021/acsomega.3c00198.

[51] C. Cui, R. Guo, H. Xiao, E. Ren, Q. Song, C. Xiang, X. Lai, J. Lan, S. Jiang, Bi_2WO_6/Nb_2CTx MXene hybrid nanosheets with enhanced visible-light-driven photocatalytic activity for organic pollutants degradation, Appl Surf Sci 505 (2020). https://doi.org/10.1016/j.apsusc.2019.144595.

[52] L. Shi, C. Xu, D. Jiang, X. Sun, X. Wang, Q. Wang, Y. Zhang, X. Qu, F. Du, Enhanced interaction in TiO_2/$BiVO_4$ heterostructures via MXene Ti_3C_2-derived 2D-carbon for highly efficient visible-light photocatalysis, Nanotechnology 30 (2019). https://doi.org/10.1088/1361-6528/aaf313.

[53] R. Long, Z. Yu, Q. Tan, X. Feng, X. Zhu, X. Li, P. Wang, Ti3C2 MXene/NH_2-MIL-88B(Fe): Research on the adsorption kinetics and photocatalytic performance of an efficient integrated photocatalytic adsorbent, Appl Surf Sci 570 (2021). https://doi.org/10.1016/j.apsusc.2021.151244.

[54] M. Han, C.E. Shuck, R. Rakhmanov, D. Parchment, B. Anasori, C.M. Koo, G. Friedman, Y. Gogotsi, Beyond Ti3C2Tx: MXenes for Electromagnetic Interference Shielding, ACS Nano 14 (2020) 5008–5016. https://doi.org/10.1021/acsnano.0c01312.

[55] H. Hu, S. Wang, Y. Zhang, X. Wang, B. Lin, S. Zhang, W. Zhang, P. Lian, MXene-Based Electromagnetic Interference Shielding Materials: A Leap From Fundamental Research to Intelligent Customization, Small n/a (n.d.) 2505417. https://doi.org/https://doi.org/10.1002/smll.202505417.

[56] R. Xu, G. Wei, Z. Xie, S. Diao, J. Wen, T. Tang, L. Jiang, M. Li, G. Hu, V2C MXene-modified g-C_3N_4 for enhanced visible-light photocatalytic activity, (n.d.).

[57] Paul Kubelka and Franz Munk, An Article on Optics of Paint Layers, Z.Tech. Phys. (1931). https://doi.org/10.1097/SLA.0000000000001706.

[58] P. Makuła, M. Pacia, W. Macyk, How To Correctly Determine the Band Gap Energy of Modified Semiconductor Photocatalysts Based on UV-Vis Spectra, Journal of Physical Chemistry Letters 9 (2018) 6814–6817. https://doi.org/10.1021/acs.jpclett.8b02892.

[59] MCNP® Website, (n.d.). https://mcnp.lanl.gov/ (accessed December 30, 2023).

[60] J.F. Briesmeister, E.T. E Booth J F Briesmeister, G.J. Collins J Devaney G P Estes H M Fisher CONTRIBUTORS R A Forster T N K Godfrey J S Hendricks H G Hughes R C Little R E Prael R G Schrandt R E Seamon E C Snow W L Thompson W T Urban J T West, MCNP-A General Monte Carlo Code for Neutron and Photon Transport, n.d.

[61] C. Data, No Title, (n.d.). https://www.crystallography.net/cod/index.php.

[62] X. Feng, Z. Yu, Y. Sun, R. Long, M. Shan, X. Li, Y. Liu, J. Liu, Review MXenes as a new type of nanomaterial for environmental applications in the photocatalytic degradation of water pollutants, Ceram Int 47 (2021) 7321–7343. https://doi.org/https://doi.org/10.1016/j.ceramint.2020.11.151.

[63] V. Soni, P. Singh, H.H. Phan Quang, A.A. Parwaz Khan, A. Bajpai, Q. Van Le, V.K. Thakur, S. Thakur, V.-H. Nguyen, P. Raizada, Emerging architecture titanium carbide (Ti_3C_2Tx) MXene based photocatalyst toward degradation of hazardous pollutants: Recent progress and perspectives, Chemosphere 293 (2022) 133541. https://doi.org/https://doi.org/10.1016/j.chemosphere.2022.133541.

[64] S. Mathew, M. Ramachandra, S.D.K. R, D. Pinheiro, S. Manickam, C.H. Pang, S.H. Sonawane, Synthesis, mechanisms, challenges, and future prospects of Ti_3C_2 MXene and its heterojunctions for photocatalytic dye degradation efficiency: a comprehensive review, Materials Today Sustainability 24 (2023). https://doi.org/10.1016/j.mtsust.2023.100568.

[65] V.Q. Hieu, T.K. Phung, T.-Q. Nguyen, A. Khan, V.D. Doan, V.A. Tran, V.T. Le, Photocatalytic degradation of methyl orange dye by Ti3C2–TiO2 heterojunction under solar light, Chemosphere 276 (2021) 130154. https://doi.org/https://doi.org/10.1016/j.chemosphere.2021.130154.

[66] M.M. Uddin, M.Z. Hossain, M.H. Kabir, S. Ghosh, M.H. Haque, M.M. Hossain, M.A. Ali, M. Akhtaruzzaman, A.M. Alanazi, S. Mondal, J. Chowdhury, D. Karmakar, D. Jana, Synergistic effects of rare-earth ions (Ho, Yb) doping on the photo-catalytic efficacy of V2O5 for removal of pollutants from industrial waste water, Heliyon

10 (2024) e37689. https://doi.org/https://doi.org/10.1016/j.heliyon.2024.e37689.

M.Phil. final thesis check

by Md. Zahid Hasan

Submission date: 06-Aug-2025 01:49AM (UTC+0600)
Submission ID: 2725740935
File name: Thesis_Zahid_Hasan_02-08-2025_edit_MU.pdf (1.77M)
Word count: 14283
Character count: 75169

M.Phil. final thesis check

ORIGINALITY REPORT

18%	13%	15%	4%
SIMILARITY INDEX	INTERNET SOURCES	PUBLICATIONS	STUDENT PAPERS

PRIMARY SOURCES

1	pubs.aip.org Internet Source	1%
2	worldwidescience.org Internet Source	1%
3	M.M. Uddin, M.Z. Hossain, M.H. Kabir, S. Ghosh et al. "Synergistic effects of rare-earth ions (Ho, Yb) doping on the photo-catalytic efficacy of V2O5 for removal of pollutants from industrial waste water", Heliyon, 2024 Publication	1%
4	bl831.als.lbl.gov Internet Source	1%
5	lib.buet.ac.bd:8080 Internet Source	<1%
6	hdl.handle.net Internet Source	<1%
7	Nadeem Hussain Solangi, Rama Rao Karri, Shaukat Ali Mazari, Nabisab Mujawar Mubarak et al. "MXene as emerging material for photocatalytic degradation of environmental pollutants", Coordination Chemistry Reviews, 2023 Publication	<1%
8	www.mdpi.com Internet Source	<1%
9	dokumen.pub Internet Source	<1%

10	export.arxiv.org Internet Source	<1 %
11	www.researchsquare.com Internet Source	<1 %
12	Submitted to Universiti Kebangsaan Malaysia Student Paper	<1 %
13	"Handbook of Ecomaterials", Springer Nature, 2019 Publication	<1 %
14	aether.cmi.ua.ac.be Internet Source	<1 %
15	G. Murali, Jeevan Kumar Reddy Modigunta, Young Ho Park, Jong-Hoon Lee, Jishu Rawal, Seul-Yi Lee, Insik In, Soo-Jin Park. "A Review on MXene Synthesis, Stability, and Photocatalytic Applications", ACS Nano, 2022 Publication	<1 %
16	M.H. Kabir, M.Z. Hossain, M.A. Jalil, S. Ghosh et al. "The efficacy of rare-earth doped V2O5 photocatalyst for removal of pollutants from industrial wastewater", Optical Materials, 2024 Publication	<1 %
17	M. A. Jalil, M. N. I. Khan, S. K. Mandal, F.-U.-Z. Chowdhury, M. M. Hossain, D. Jana, M. S. Alam, M. M. Uddin. " Impact of reaction temperatures on the particle size of V O synthesized by facile hydrothermal technique and photocatalytic efficacy in dye degradation ", AIP Advances, 2023 Publication	<1 %
18	Lijun Nie, Yuhang Gao, Kunkun Xue, Na Zheng, Wangchao Su, Yueyu Ma, Xiaobei Han,	<1 %

	Lirong Ren, Jianhui Shi, Cyrille Boyer. "Floating PVDF/CQDs/g-C3N4 photocatalytic composite membrane with pyroelectric effect for effective degradation of dyes from wastewater under broad light spectrum", Colloids and Surfaces A: Physicochemical and Engineering Aspects, 2025 Publication	
19	"Fundamental Aspects and Perspectives of MXenes", Springer Science and Business Media LLC, 2022 Publication	<1 %
20	kups.ub.uni-koeln.de Internet Source	<1 %
21	ltu.diva-portal.org Internet Source	<1 %
22	mdpi-res.com Internet Source	<1 %
23	research.polyu.edu.hk Internet Source	<1 %
24	www.frontiersin.org Internet Source	<1 %
25	Zakarya Othman, Alessandro Sinopoli, Hamish R. Mackey, Khaled A. Mahmoud. " Efficient Photocatalytic Degradation of Organic Dyes by AgNPs/TiO /Ti C T MXene Composites under UV and Solar Light ", ACS Omega, 2021 Publication	<1 %
26	scholarworks.iupui.edu Internet Source	<1 %
27	wiki.anton-paar.com Internet Source	<1 %

28	Wee-Jun Ong, Lling-Lling Tan, Yun Hau Ng, Siek-Ting Yong, Siang-Piao Chai. " Graphitic Carbon Nitride (g-C N)-Based Photocatalysts for Artificial Photosynthesis and Environmental Remediation: Are We a Step Closer To Achieving Sustainability? ", Chemical Reviews, 2016 Publication	<1 %
29	www.nature.com Internet Source	<1 %
30	Ashish Garg, Neeraj Mishra, Vikas Pandey, Sabapathi Mohana Lakshmi. "Metallic Nanoparticles in Cancer Therapy - Synthesis, Applications, and Regulatory Considerations", CRC Press, 2025 Publication	<1 %
31	link.springer.com Internet Source	<1 %
32	"2D Metal Carbides and Nitrides (MXenes)", Springer Science and Business Media LLC, 2019 Publication	<1 %
33	Submitted to Higher Education Commission Pakistan Student Paper	<1 %
34	coek.info Internet Source	<1 %
35	helmholtz-berlin.de Internet Source	<1 %
36	www.idosi.org Internet Source	<1 %
37	Bendi Anjaneyulu, Vishaka Chauhan, Chanchal Vashisth, Yogita, Chinmay, Neera	<1 %

Raghav. "Revolutionizing industrial wastewater Treatment: MXenes conquer organic pollutants in a paradigm shifting breakthrough towards Sustainability", Chemical Engineering Journal, 2024
Publication

38	Submitted to Dublin City University Student Paper	<1 %
39	pubs.rsc.org Internet Source	<1 %
40	ulspace.ul.ac.za Internet Source	<1 %
41	www.osti.gov Internet Source	<1 %
42	Submitted to Queen Mary and Westfield College Student Paper	<1 %
43	tudr.thapar.edu:8080 Internet Source	<1 %
44	"Ferroelectric Materials for Energy Applications", Wiley, 2018 Publication	<1 %
45	Basiru O. Yusuf, Mustapha Umar, Mansur Aliyu, Aliyu M. Alhassan et al. "Recent advances and future prospects of MXene-based photocatalysts in environmental remediations", Journal of Environmental Chemical Engineering, 2024 Publication	<1 %
46	Ji Yoon Kim, M. S. Balathanigaimani, Hee Moon. "Adsorptive Removal of Nitrate and Phosphate Using MCM-48, SBA-15, Chitosan,	<1 %

and Volcanic Pumice", Water, Air, & Soil Pollution, 2015
Publication

47	Durkee, Joe W., Russell C. Johns, and Laurie S. Waters. "MCNP6 moving objects part I: Theory", Progress in Nuclear Energy, 2016. Publication	<1 %
48	Submitted to Imperial College of Science, Technology and Medicine Student Paper	<1 %
49	Muhammad Azam Qamar, Sally Mostafa Khadrawy, Ahmed A. Allam, Syed Kashif Ali et al. "A comprehensive review on advanced synthesis approaches of MXenes and their dual role in photocatalytic degradation and antimicrobial applications", Reviews in Inorganic Chemistry, 2025 Publication	<1 %
50	Submitted to Universiti Putra Malaysia Student Paper	<1 %
51	www.theses.fr Internet Source	<1 %
52	"Semiconductors", Springer Science and Business Media LLC, 2019 Publication	<1 %
53	Ali Mohammad Amani, Milad Abbasi, Atena Najdian, Farzaneh Mohamadpour et al. "A potentially fruitful path toward a cleaner and safer environment: MXenes uses in environmental remediation", Ecotoxicology and Environmental Safety, 2025 Publication	<1 %
54	Hewitt, David Jason. "MCNP Design of Radiation Shielding for Pulsed Fusion	<1 %

Propulsion.", The University of Alabama in Huntsville, 2020
Publication

55	Jarrett, John Michael. "Experimental Method Development for Direct Dosimetry of Permanent Interstitial Prostate Brachytherapy Implants", Louisiana State University and Agricultural & Mechanical College, 2022 Publication	<1 %
56	Shridhar Hegde, Hafis Hakkeem, Srinivasan Alagar, Erdenebayar Baasanjav, Chandra Sekhar Rout, Sang Mun Jeong. "Laser-driven engineering of modulated structural defects in Nb2CTx MXene-rGO based flexible microsupercapacitors for energy storage application", Journal of Energy Storage, 2025 Publication	<1 %
57	Submitted to University of Leicester Student Paper	<1 %
58	Zeynep Kalaycıoğlu, Bengü Özuğur Uysal, Önder Pekcan, F. Bedia Erim. "Efficient Photocatalytic Degradation of Methylene Blue Dye from Aqueous Solution with Cerium Oxide Nanoparticles and Graphene Oxide-Doped Polyacrylamide", ACS Omega, 2023 Publication	<1 %
59	arxiv.org Internet Source	<1 %
60	mafiadoc.com Internet Source	<1 %
61	www.texilajournal.com Internet Source	<1 %
62	Luyao Wang, Hongru Jiang, Hui Wang, Pau Loke Show, Andrei Ivanets, Dan Luo,	<1 %

Chongqing Wang. "MXenes as heterogeneous Fenton-like catalysts for removal of organic pollutants: A review", Journal of Environmental Chemical Engineering, 2022
Publication

63	Pascaline Sanga, Haitham Saad Al-mashriqi, Jing Xiao, Jia Chen, Hongdeng Qiu. "Streamlined fabrication of AuPtRh trimetallic nanoparticles supported on Ti3C2MXene for enhanced photocatalytic activity in cephalosporins degradation", Journal of Colloid and Interface Science, 2023 Publication	<1 %
64	www.ijitee.org Internet Source	<1 %
65	Adem Sreedhar, Jin-Seo Noh. "Role of emerging 2D Nb2CTx MXene for multiple toxic matter degradation, H2 generation, and H2 storage applications: A review", Journal of Water Process Engineering, 2025 Publication	<1 %
66	Huoli Zhang, Man Li, Jianliang Cao, Qingjie Tang, Peng Kang, Changxin Zhu, Mingjie Ma. "2D a-Fe 2 O 3 doped Ti 3 C 2 MXene composite with enhanced visible light photocatalytic activity for degradation of Rhodamine B", Ceramics International, 2018 Publication	<1 %
67	Jing Jiang, Kun Zhao, Xiaoyi Xiao, Lizhi Zhang. "Synthesis and Facet-Dependent Photoreactivity of BiOCl Single-Crystalline Nanosheets", Journal of the American Chemical Society, 2012 Publication	<1 %

68	M. A. Jalil, M. N. I. Khan, S. K. Mandal, F.-U.-Z. Chowdhury, M. M. Hossain, D. Jana, M. S. Alam, M. M. Uddin. "Impact of reaction temperatures on the particle size of V2O5 synthesized by facile hydrothermal technique and photocatalytic efficacy in dye degradation", AIP Advances, 2023 Publication	<1 %
69	Wendorff, Carl. "Validation and Benchmarking of the Thermal Neutron Scattering Law Data Files for Neutron Moderators Using Experimental Data.", Rensselaer Polytechnic Institute, 2019 Publication	<1 %
70	Zakarya Othman, Hamish R. Mackey, Khaled A. Mahmoud. "A critical overview of MXenes adsorption behavior toward heavy metals", Chemosphere, 2022 Publication	<1 %
71	nano.materials.drexel.edu Internet Source	<1 %
72	repository.um-palembang.ac.id Internet Source	<1 %
73	ubm.opus.hbz-nrw.de Internet Source	<1 %
74	www.ir.nctu.edu.tw Internet Source	<1 %
75	www.rsc.org Internet Source	<1 %
76	www.tandfonline.com Internet Source	<1 %
77	Submitted to Botswana International University of Science and Technology	<1 %

Student Paper

78	Hala M. Abo-Dief, Omima K. Hussein, Ayesha Ihsan, Salah M. El-Bahy, Asmaa M. Raslan, Muhammad Shahid, Muhammad Farooq Warsi. "Ternary metal oxide WO3.NiO.ZnO nanoparticles and their composite with CNTs for organic dye photocatalytic degradation", Ceramics International, 2022 Publication	<1 %
79	Kirill Fedorov, Manoj P. Rayaroth, Noor S. Shah, Grzegorz Boczkaj. "Activated sodium percarbonate-ozone (SPC/O3) hybrid hydrodynamic cavitation system for advanced oxidation processes (AOPs) of 1,4-dioxane in water", Chemical Engineering Journal, 2022 Publication	<1 %
80	Mohammed Abualsayyed, M. Kh Hamad, M.H.A. Mhareb, Nimitha S. Prabhu, Hossein Khosravi, Sudha D. Kamath. "Effect of different modifiers on mechanical and radiation shielding properties of SrO-B2O3-TeO2 glass system", Optik, 2022 Publication	<1 %
81	Submitted to University of Nigeria Student Paper	<1 %
82	Yuxi Zhang, Kuangjun Li, Meng Zang, Yuanyuan Cheng, Hongbin Qi. "Graphene-based photocatalysts for degradation of organic pollution", Chemosphere, 2023 Publication	<1 %
83	acikbilim.yok.gov.tr Internet Source	<1 %
84	etheses.whiterose.ac.uk Internet Source	<1 %

85	libjncir.jncasr.ac.in Internet Source	<1 %
86	repository.biust.ac.bw Internet Source	<1 %
87	vdoc.pub Internet Source	<1 %
88	wiredspace.wits.ac.za Internet Source	<1 %
89	www.hindawi.com Internet Source	<1 %
90	www.samaterials.com Internet Source	<1 %
91	www.science.org Internet Source	<1 %
92	www.thefreelibrary.com Internet Source	<1 %
93	Adem Sreedhar, Jin-Seo Noh. "Recent advances in partially and completely derived 2D Ti3C2 MXene based TiO2 nanocomposites towards photocatalytic applications: A review", Solar Energy, 2021 Publication	<1 %
94	Adjei, Christian A. "MCNP5 and GEANT4 comparisons for preliminary Fast Neutron Pencil Beam design at the University of Utah TRIGA system", Proquest, 2014. Publication	<1 %
95	C. Akshhayya, Mohammad K. Okla, Abdullah A. Al-ghamdi, Saud A. Al-amri et al. "Nano-architecture of Intimate n-CuFe2O4 Coupled p-NiO for Enhanced White Light	<1 %

Photocatalysis: Kinetics and Intrinsic Mechanism", Journal of Cluster Science, 2022
Publication

96	Chuanfeng Zang, Xiangye Han, Hao Chen, Haifeng Zhang, Yonggang Lei, Hongchao Liu, Guangyu Zhang, Mingzheng Ge. "In situ growth of ZnO/Ag2O heterostructures on PVDF nanofibers as efficient visible-light-driven photocatalysts", Ceramics International, 2022 Publication	<1 %
97	D. Sangamithirai, S. Ramanathan. "Electrochemical Sensing Platform for the Detection of Nitroaromatics Using g-C3N4/V2O5 Nanocomposites Modified Glassy Carbon Electrode", Electrochimica Acta, 2022 Publication	<1 %
98	Dan Xu, Yuwei Hua, Yanyan Huang, Yiming Zhao et al. "Synergistic adsorption and Fenton-like oxidation of neutral red by the combination of COFs and Co(OH)2 in chitosan hydrogel microspheres", Sustainable Materials and Technologies, 2025 Publication	<1 %
99	Dikra Bouras, Lotfi Khezami, Regis Barille, Neçar Merah, Billel Salhi, Gamal A. El-Hiti, Ahlem Guesmi, Mamoun Fellah. "Preparation Methods and Photocatalytic Performance of Kaolin-Based Ceramic Composites with Selected Metal Oxides (ZnO, CuO, MgO): A Comparative Review", Inorganics, 2025 Publication	<1 %
100	Ghada AlMisned, Duygu Sen Baykal, Hessa Alkarrani, Gulfem Susoy, H.O. Tekin. "Advancing mechanical durability and	<1 %

radiation shielding properties in Silicon dioxide (SiO2) glasses through various incorporations: A comparative analysis", Results in Physics, 2024
Publication

---

101 Jarosław Serafin, Bartosz Dziejarski, George Oindo Achieng, Xavier Vendrell, Stefanos Chaitoglou, Roger Amade-Rovira. "Comprehensive analysis of MAX phase and MXene materials for advanced photocatalysis, electrocatalysis and adsorption in hydrogen evolution and storage", Journal of Industrial and Engineering Chemistry, 2024 <1 %
Publication

---

102 Mahmoud A. Ahmed, Safwat A. Mahmoud, Ashraf A. Mohamed. "Insights into MXene-based materials for environmental applications: Performance, mechanisms, and future directions", FlatChem, 2025 <1 %
Publication

---

103 Nan Xu, Wei Wang, Zhijia Zhu, Chunyan Hu, Baojiang Liu. "Recent developments in photocatalytic water treatment technology with MXene material: A review", Chemical Engineering Journal Advances, 2022 <1 %
Publication

---

104 Weixue Meng, Xingjiang Liu, Haoqiang Song, Yu Xie, Xiaolei Shi, Matthew Dargusch, Zhi-Gang Chen, Zhiyong Tang, Siyu Lu. "Advances and challenges in 2D MXenes: From structures to energy storage and conversions", Nano Today, 2021 <1 %
Publication

---

105 X. Wang, C. Garnero, G. Rochard, D. Magne et al. " A new etching environment (FeF /HCl) for <1 %

	the synthesis of two-dimensional titanium carbide MXenes: a route towards selective reactivity vs.water ", J. Mater. Chem. A, 2017 Publication	
106	Y.M. Hunge, A.A. Yadav, Seok-Won Kang, Hyunmin Kim. "Photocatalytic degradation of tetracycline antibiotics using hydrothermally synthesized two-dimensional molybdenum disulfide/titanium dioxide composites", Journal of Colloid and Interface Science, 2022 Publication	<1 %
107	addi.ehu.es Internet Source	<1 %
108	arts.units.it Internet Source	<1 %
109	dokumen.tips Internet Source	<1 %
110	ebin.pub Internet Source	<1 %
111	eprints.nottingham.ac.uk Internet Source	<1 %
112	etd.adm.unipi.it Internet Source	<1 %
113	kyutech.repo.nii.ac.jp Internet Source	<1 %
114	openaccess.iyte.edu.tr Internet Source	<1 %
115	research-information.bris.ac.uk Internet Source	<1 %
116	www.eurasianbiochem.org Internet Source	<1 %
	www.isres.org	

117	Internet Source	<1%
118	www.psi.ch Internet Source	<1%
119	www.sssihl.edu.in Internet Source	<1%

Exclude quotes	On	Exclude matches	< 8 words
Exclude bibliography	On		